RSC Advances

PAPER

View Article Online
View Journal | View Issue

Cite this: *RSC Adv.*, 2021, **11**, 29466

A multi-colorimetric probe to discriminate between heavy metal cations and anions in DMSO–H_2O with high selectivity for Cu^{2+} and CN^-: study of logic functions and its application in real samples†

Eunike Hamukwaya, Johannes Naimhwaka and Veikko Uahengo *

A ditopic multi-colorimetric probe based on the phenylpridyl-thioic moiety (**EN**) was synthesized *via* a Schiff base reaction mechanism and characterized using ^{1}H NMR and UV-vis spectroscopy. The colorimetric analyses carried out revealed that **EN** was capable of discriminating between a number of heavy metal cations *via* coordination induced charge transfer, as well as between anions through hydrogen bonding induced charge transfer, in DMSO–H_2O (9 : 1). In particular, the ditopic probe could spectrally and colorimetrically recognize the most toxic heavy metal cations of Cd^{2+}, Pb^{2+} and Hg^{2+}, among others, in DMSO–H_2O. Additionally, **EN** was selective and sensitive to the presence of CN^-, F^-, AcO^- and $H_2PO_4^-$ in the same solvent system as cations. The reversibility and reproducibility studies showed that **EN** exhibited complementary IMP/INH logic functions, based on colour and spectral switching (ON/OFF), modulated by F^-/Al^{3+}. The real time application of the probe was tested on food grade products to detect the presence of F^- in toothpastes and mouthwash dissolved in water, as well as cations in underground water (normally saline), which displayed substantial responses. Thus, **EN** displayed an excellent scope of response and can thus be developed for real time sensing kits, which could be used instantly in on-field analysis. Theoretical studies were conducted to complement the experimental work.

Received 18th June 2021
Accepted 4th August 2021

DOI: 10.1039/d1ra04734e

rsc.li/rsc-advances

1. Introduction

Diagnostic chemistry techniques have taken center stage for many research groups around the globe in recent decades, perpetuated by the complexity of the chemical effluents off-loaded into environmental systems nowadays. These effluents are the result of the rapid increase in the technology dependency of contemporary societies, especially in the agricultural and telecommunication sectors, to meet the demand of food production and communication technology, respectively, to supply the increasing global population.[1–4] Thus, most of these new technologies depend on the use of chemicals in their manufacture and function, which in most cases end up in environmental streams. Chemicals are classified as the most toxic pollutants on the face of the earth, thus their threshold concentration levels must be controlled and monitored. Traditional analytical methods such as inductive coupled plasma (ICP) and atomic absorption spectroscopy (AAS) have become obsolete and too expensive to afford, let alone that they are inconveniently time-consuming.[5–9] Subsequently, the development of new analytical methods has been the focal center of many research groups in the world to combat the threat of environmental pollutants. Thus, chemosensing has been identified as one of the potential analytical methods used in sensing the presence of cations (mostly heavy metals) and anions in physiological and environmental systems, instead of traditional methods.[10–16]

Chemosensing has become a method of choice in analytical chemistry as it is sensitive and selective to specific target analytes which are ionic or neutral, depending on the design of the sensor.[17–27] This is complemented by the fact that they are easily synthesized, easy to apply, can be applied in real time and are based on naked eye observable colour changes. The structural frameworks of chemosensors are designed with in-built specific features, bearing a receptor, relay and reporter (3R). To date, numerous colorimetric and fluorometric probes for both cations and anions have been reported in the literature, some of which are on the market already.[13,28–30] The chemical phenomenon of the sensing process is founded on charge transfer mechanisms such as intramolecular charge transfer (ICT), excited state intermolecular proton transfer (ESIPT), photoinduced charge transfer (CT) and metal-to-ligand charge transfer (MLCT), among others.[31–36] For cations, the sensing mechanism is normally governed by coordination induced charge transfer, while the hydrogen bonding induced charge transfer

Department of Chemistry and Biochemistry, University of Namibia, 340 Mandume Ndemufayo Avenue, Windhoek, 9000, Namibia. E-mail: vuahengo@unam.na; vuahengo@gmail.com; Tel: +264 61 206 3465

† Electronic supplementary information (ESI) available. See DOI: 10.1039/d1ra04734e

mechanism is common for anions. Notably, the structural framework of probes which are sensitive and selective for anions are usually characterized by amine,[37,38] hydroxyl,[39] sulfonyl,[40] urea[41,42] and hydrazone[43–45] groups, while cation probes normally bear soft donor atoms such as oxygen, nitrogen and sulfur. However, there are other interaction mechanisms, governed by weak Van der Waals forces, which can induce the sensing of cations and anions.[46,47]

Probes which are sensitive and selective to cations (heavy metals) such as copper (Cu^{2+}), mercury (Hg^{2+}), zinc (Zn^{2+}), iron (Fe^{3+}) and to some extent nickel (Ni^{2+}) are fairly commonly reported in the literature, however, colorimetric sensors for highly toxic cations such as lead (Pb^{2+}), tin (Sn^{2+}), cobalt (Co^{2+}), cadmium (Cd^{2+}), iron (Fe^{2+}) and silver (Ag^{+}) are rarely reported.[12,23,48–51] Notably, the presence of too high or too low quantities of specific cations in physiological or environmental systems results in severe adverse effects, which lead to disruption in physiological homeostasis. Furthermore, just like cations, anion sensors for common ions such as fluoride (F^-), acetate (AcO^-) and dihydrogen phosphate ($H_2PO_4^-$) have been heavily reported, however, highly toxic anions such as cyanide (CN^-), cyanate (OCN^-) and hydroxide (OH^-) remain subjects of interest.[28,52–55] The nature of sensors varies with structural designs based on the target analytes, and single and dual sensors can be developed,[56–63] including ditopic-based sensors; however, multifunctional sensors have been rarely been reported in the literature and remain a subject of high priority.[64–66] Thus, in this study, a ditopic multifunctional colorimetric sensor (**EN**) based on the pyridyl-thioic moiety was synthesized (Scheme 1) which could discriminate between a series of cations, including Pb^{2+}, Sn^{2+} and Hg^{2+}, among others, as well as anions of CN^-, F^- and OH^-, among others. In addition, reversibility and reproducibility studies were carried out, concluding that **EN** exhibited logic functions (INH/IMP).[22,67,68] The solvatochromic affect was also conducted in order to study and investigate the optoelectronic properties of **EN**, which shed more light on the dye sensitizing properties, a subject of interest to our group.

2. Experimental section

2.1 Materials and apparatus

All reagents and solvents were commercially available and of analytical grade. They were used without further purification unless stated. UV-vis spectroscopy was performed with a Perkin Elmer Lambda 35 spectrophotometer in a standard 3.0 ml quartz cuvette with a 1 cm path length. ^{1}H NMR spectra were recorded on a Varian Mercury VX-300 MHz spectrometer in CD_3CN. Elemental analyses (C, H and N) were carried out on a Perkin Elmer 240C analytical instrument. All of the measurements were conducted at ambient temperature (25 °C).

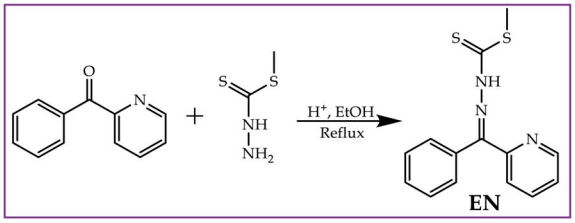

Scheme 1 Synthetic procedure for **EN**.

2.2 General procedure for the UV-vis experiments

All UV-vis spectra were recorded in DMSO–H_2O (9 : 1) on a Perkin Elmer Lambda 35 spectrometer after the addition of tetrabutylammonium salts while keeping the sensor **EN** concentration constant (1×10^{-5} M). Tetrabutylammonium salts (TBA) of the anions (F^-, Cl^-, Br^-, I^-, AcO^-, CN^-, OH^-, $H_2PO_4^-$ and ClO_4^-) were used for the UV-vis experiments. TBA salts of the anions (F^-, Cl^-, Br^-, OH^-, I^-, AcO^-, $H_2PO_4^-$, ClO_4^- and CN^-) were used for the fluorescence experiments.

2.3 Job plot experiments

Stoichiometric interactions were determined using a Job plot by preparing solutions of TBAAcO and $Cu(NO_3)_2$ (1×10^{-4} M) in DMSO–H_2O at ambient temperature. Each solutions of these were mixed with the standard solution of **EN** (1×10^{-4} M) with volumetric/molar variations from 0 to 10 ml, then the absorbance of each solution was measured. The process was conducted for all mixing ratios of the host–guest combinations from 1 to 9.

2.4 Synthetic procedure

An ethanolic solution (15 ml) of 2-benzoylpyridine [1.0 g; 0.005 mol] was drop-wise mixed with a solution (15 ml) of methyl hydrazinecarbodithioate (1.0 g; 0.005 mol) while being magnetically stirred and catalyzed with a few drops of acetic acid. The solution mixture was refluxed for up to 3 hours before a brown precipitate appeared. The brown precipitate was then filtered off and washed several times with hot ethanol. The product was dried in a vacuum at room temperature and recrystallized from ethanol. Yield 82%. ^{1}H NMR (400 MHz, DMSO-d_6) δ 14.41 (d, $J = 7.4$ Hz, 1H), 8.88 (d, $J = 5.5$ Hz, 1H), 8.10–7.90 (m, 1H), 7.70–7.39 (m, 7H) (Fig. S4†). Elemental analysis calcd (%) for C: 58.51, H: 4.56, N: 14.62, S: 22.31; found: C: 59.22, H: 5.13, N :14.07, S: 23.13.

3. Results and discussions

3.1 Photophysical properties of EN

The absorption spectrum of **EN** was characterized by two prominent absorption peaks, both in the UV region (Fig. 1) at 282 nm and 353 nm, in DMSO–H_2O. The spectrum exhibited a low energy band at 282 nm which was ascribed to the localized π–π^* transitions, while a high-energy band at 383 nm was due to the charge transfer bands, at times mixed with a more delocalized π–π^* transition (Fig. 1).[69–71] An absorption band near the visible light region (353 nm) of the spectrum is normally a good indicator for potential dye sensitizers when subjected to the judicious tuning of the optoelectronic properties, such as solvatochromism or any other methods, thus **EN** can be tuned into a potential organic dye sensitizer for application in

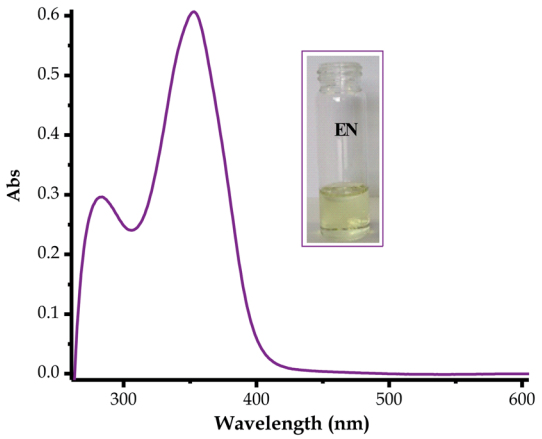

Fig. 1 Absorption spectrum of **EN** (1×10^{-5} M) in DMSO–H_2O.

solar cells.[72–74] The absorption spectrum of **EN** was accompanied by a light yellow colour (Fig. 1 inset), complementing the characteristics of the transitions in the UV region. Moreover, the optoelectronic properties of **EN** are closely linked to the chemosensing process, as both are governed by the same charge transfer mechanism (ICT), which tunes it into a multifunctional dye molecule.

3.2 Chemosensing property studies

3.2.1 Cation sensing properties. The molar addition of most transition metal salts (nitrates and chlorides) to **EN** was investigated and observed by the naked eye observable colour changes for each metal cation added (Fig. 2). The sensor could sense a variety of transition metals ranging from M^{II} to M^{III} valencies, as displayed by the number of molar additions which induced colour changes upon interacting. Upon reacting **EN** with Sn^{2+}, the colour could be observed to change from light yellow to intense yellow. The colour changes were: Ni^{2+} (intense yellow), Pb^{2+} (yellow), Hg^{2+} (yellow), Ag^{+} (intense yellow), Zn^{2+} (yellow), Co^{2+} (orange-yellowish), Fe^{3+} (yellow) and Cu^{2+} (yellow-greenish) as shown in (Fig. 2). The only additions of the cations used that did not induce any colour change were for Cr^{3+} and Al^{3+} (Fig. 2), which perhaps indicates that no chemical interaction was taking place between **EN** and both of these trivalent cations. Moreover, the colour changes are associated with the chelation-induced activities upon cations binding with **EN**.

In addition to the colorimetric changes observed, the molar addition of cations to **EN** was further observed by UV-vis titrations in DMSO–H_2O solvent mixture (9 : 1). Upon the gradual volumetric and molar equivalent addition of Pb^{2+} (nitrate salt) in DMSO–H_2O to **EN**, the absorption band at 353 nm decreased in intensity, while the initial low energy band at 253 nm was gradually enhanced with blue shift characteristics (Fig. 3a). Furthermore, the hypochromic shift experienced at 353 nm was concomitantly observed with a new broad band in the visible region, extended from 400 to slightly over 450 nm (Fig. 3a), which was assigned to the coordination induced charge transfer between **EN** and Pb^{2+} in the particular solvent system used. As expected, the absorption spectral changes observed upon the introduction of Pb^{2+} to **EN** were in agreement with the naked eye observable colour changes from light yellow to intense yellow (Fig. 2). The union of two species (**EN** and **EN–Pb**) co-existing in one system was confirmed by the two isosbestic points at 297 nm and 384 nm.[75] In addition to **EN–Pb**, the dye was further investigated for the recognition of other cations to confirm the naked eye colorimetric observations and it turned out that **EN** was further selective and sensitive to the presence of Sn^{2+} (**EN–Sn**), Ag^{+} (**EN–Ag**), Hg^{2+} (**EN–Hg**), Co^{2+} (**EN–Co**) and Cu^{2+} (**EN–Cu**), as shown in Fig. 3a–f, respectively, with their titration profiles presented in the insets.

Furthermore, the multifunctional sensing ability of **EN** was observed across nearly the entire 3d transition metal row, with Ni^{2+} (**EN–Ni**), Zn^{2+} (**EN–Zn**), Fe^{2+} (**EN–Fe(II)**) and Fe^{3+} (**EN–Fe(III)**) again inducing remarkable spectral changes, in addition to colorimetric changes in DMSO–H_2O, as shown in Fig. 4a–d, respectively, with their titration profiles shown in the insets. Commonly, the addition of these cations was characterized by the disappearance of a high energy band at 353 nm concomitantly with the appearance of a new band with observable maxima at 440 nm (Ni^{2+}), 400 nm (Zn^{2+}), 422 nm (Cu^{2+}) and 434 nm (Co^{2+}), as shown in Fig. 3 and 4. However, the band at 253 nm showed mixed changes, decreasing for Sn^{2+} while increasing for all of the other cations used. The variation in the spectral displays is the result of the differences in the interactions and associations of the cations with **EN** and the geometrically complementary nature of the complexed states. Interestingly, different valencies (Fe^{2+} and Fe^{3+}) exhibited different chemical associations with **EN**, as evidenced by their respective spectra (Fig. 4c and d). The spectra of Fe^{2+} and Fe^{3+} attest that the nature of their interactions with **EN** are completely different, thus resulting in distinctive spectra. In summary, the colorimetric changes displayed after the addition of different cations are all (apart from Fe^{3+}) corresponding to the disappearance of π–π^* transitions upon the addition of the

Fig. 2 Observable colorimetric changes of the cations (0.03 M) upon interacting with **EN** (1×10^{-5} M) in DMSO–H_2O at room temperature.

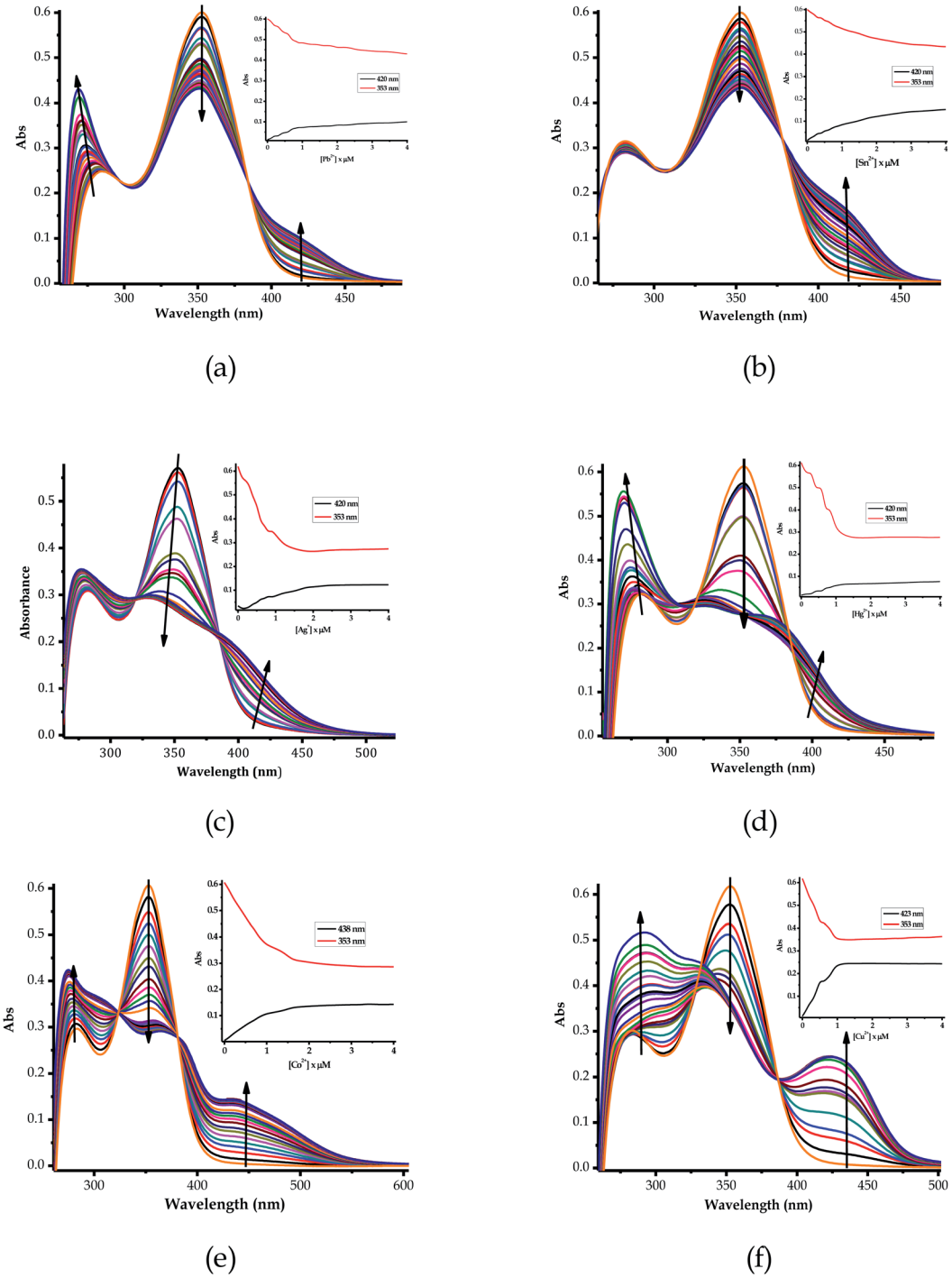

Fig. 3 The absorption titration spectra of **EN** (1×10^{-5} M) in DMSO–H_2O upon the addition of 5 equiv. of (a) Pb^{2+}, (b) Sn^{2+}, (c) Ag^{+}, (d) Hg^{2+}, (e) Co^{2+} and (f) Cu^{2+} (0.03 M) at room temperature, with their titration profiles shown in the insets.

cations, while a charge transfer band appeared in the visible region, at the same time accompanied by change in the colour. The transmission of **EN** in the presence of cations is attributed to the coordination or chelation induced mechanisms through the electron donors of sulfur and nitrogen built into the structural framework of **EN**. A few cations could not induce any noticeable change either spectrally or colorimetrically (Fig. S1†).

3.2.2 Anion sensing properties. The addition of anionic salts (tetrabutylammonium salts) to **EN** was markedly accompanied by naked eye observable colour changes, with the change in colours based on the individual anions added (Fig. 5). Precisely, the addition of F^{-}, CN^{-}, OH^{-} (slight), AcO^{-} and $H_2PO_4^{-}$ to **EN** (light yellow in colour) resulted in colour changes ranging from yellow to intense yellow (Fig. 5) in DMSO–H_2O. The colorimetric activities are ascribed to the hydrogen bonding

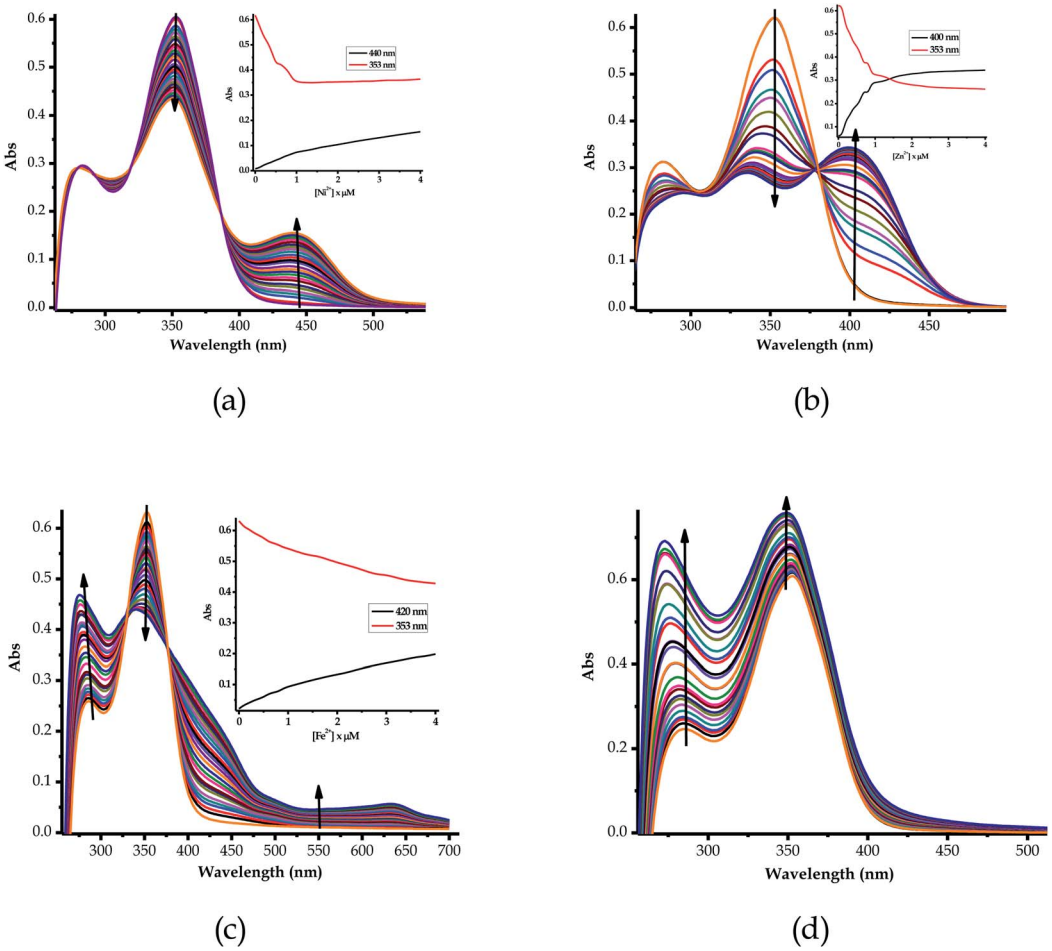

Fig. 4 The absorption titration spectra of **EN** (1×10^{-5} M) in DMSO–H_2O upon the addition of 5 equiv. of (a) Ni^{2+}, (b) Zn^{2+}, (c) Fe^{2+} and (d) Fe^{3+} (0.03 M) at room temperature, with their titration profiles shown in the insets.

induced interaction between **EN** and the anions. Normally, the interaction with anions is expedited through the amide proton –NH group of **EN** upon encountering the negatively charged anions. In addition to the anions recognized (F^-, CN^-, OH^-, AcO^- and $H_2PO_4^-$), the molar titration using other anions (Cl^-, Br^-, I^-, NO_3^-, N_3^-, HSO_4^- and ClO_4^-) added to **EN** did not induce any significant colour changes.

The color change activities observed were verified by spectroscopic analysis using UV-vis titrations in DMSO–H_2O. For instance, upon the molar addition of $H_2PO_4^-$ (TBA salt) to **EN**, the main absorption band at 354 nm went through a hypochromic shift, which was concomitant with the appearance of a new band in at 394 nm (Fig. 6a). The probe (**EN**) experienced a bathochromic shift of 40 nm, which was ascribed to intermolecular charge transfer caused by the interaction between **EN** and $H_2PO_4^-$. Distinctively, the co-existence of two different species (**EN** and **EN–H_2PO_4**) in one system at equilibrium was confirmed by the isosbestic points at 266 nm, 302 nm and 376 nm. Other anions which displayed colorimetric activities upon addition to **EN** were spectroscopically investigated, whereby similar spectral behaviors to those of **EN–H_2PO_4** were observed for other anions (F^-, CN^-, OH^- (slight) and AcO^- (Fig. 6b–d, respectively), signifying similar chemical associations with **EN**. In each case, the titration profiles are given in the insets of Fig. 6. The molar titration of F^-, CN^- and AcO^- with **EN** resulted in the same effect as $H_2PO_4^-$, resulting in the

Fig. 5 Observable colorimetric activities of different anions (0.03 M) upon interacting with **EN** (1×10^{-5} M) in DMSO–H_2O at room temperature.

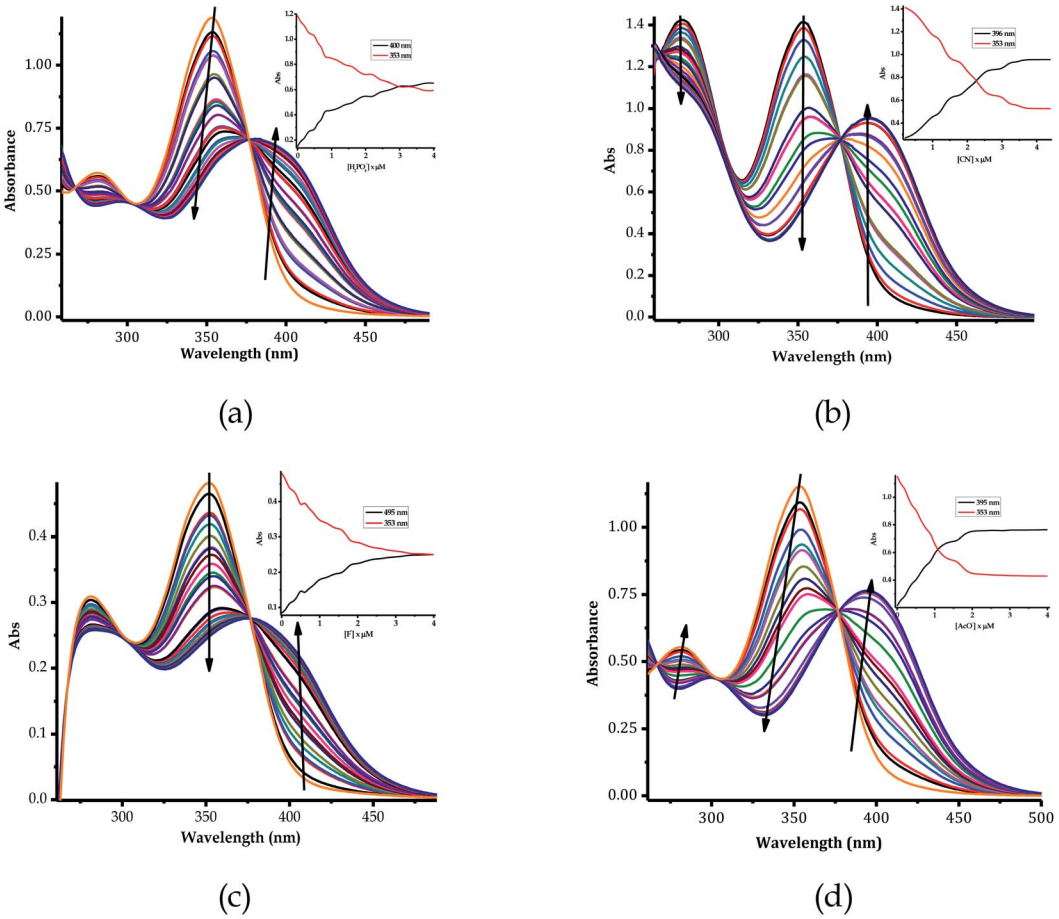

Fig. 6 The absorption titration spectra of **EN** (1×10^{-5} M) in DMSO–H_2O, upon the addition of 5 equiv. of (a) $H_2PO_4^-$, (b) CN^-, (c) F^- and (d) AcO^- (0.03 M) at room temperature, with their titration profiles shown in the insets.

disappearance of the π–π* transition band at 354 nm concomitantly with the appearance of a new intermolecular charge transfer band at 394 nm, with the isosbestic point at 376 nm (Fig. 6b–c). In contrast, the molar addition of OH^- to **EN** induced slight spectral changes, proposed to be the result of a weaker complexed state of **EN–OH**, compared to the rest of the anions used (Fig. S2†).

3.3 Job plots and the binding modes of EN with cations and anions

Furthermore, to understand the interactions and binding modes of **EN** towards the anions and cations, the Job plots for selected species were carried out (Fig. 7). The molecular recognition of cations is normally by the coordination mechanism, facilitated by the presence of donor atoms in the structural framework of the sensor. Thus, it was expected that cation recognition by **EN** was potentially enabled through the nitrogen and sulfur atoms in the structure. Upon running the Job plot, the results projected that the interaction mode involved at least two sensor molecules to one cation, thus signifying a 2 : 1 (2**EN** : 1Cu) interaction ratio. Thus, for instance, **EN** interacts with Cu^{2+} in a 2 : 1 binding ratio, as displayed in Fig. 7a, and the binding is roughly predicted to be through the nitrogen atoms in the sandwich scaffold (Fig. 7b). This prediction was reached as a result of obtaining the maximum value at a molar fraction of 3 (with a possibility of 3.5), signifying a 2 : 1 ratio. An admixture solution may be possible, which could contain a 1 : 1 and a predominantly 2 : 1 mixture, based on the mole ratio absorption maxima of the spectrum.

The interaction of **EN** with the anions is by a hydrogen bonding mechanism by default, through the –NH proton in the structure. Thus, the presence of one –NH group in the structure of the probe (**EN**) was a good indicator to predict the nature of the interaction and the binding mode, which was likely to be in a 1 : 1 (**EN** : **A**) ratio. Consequently, the Job plot analysis conducted was in agreement with the prediction, where AcO^- associates with **EN** in a 1 : 1 interaction (Fig. 7c) and the projected interaction is through the –NH group, as indicated in Fig. 7d. In addition to the interaction with AcO^-, the other anions (F^- and CN^-) sensed are predicted to interact in a similar way with a 1 : 1 binding mode. The information was extracted from the data plot and the maximum absorption of the spectrum was at a molar fraction of 0.5, which was suggestive of a 1 : 1 ratio. Moreover, the limits of detection (LOD) were determined with data extracted from the UV-vis analysis of the titration profiles. The absorbance was recorded

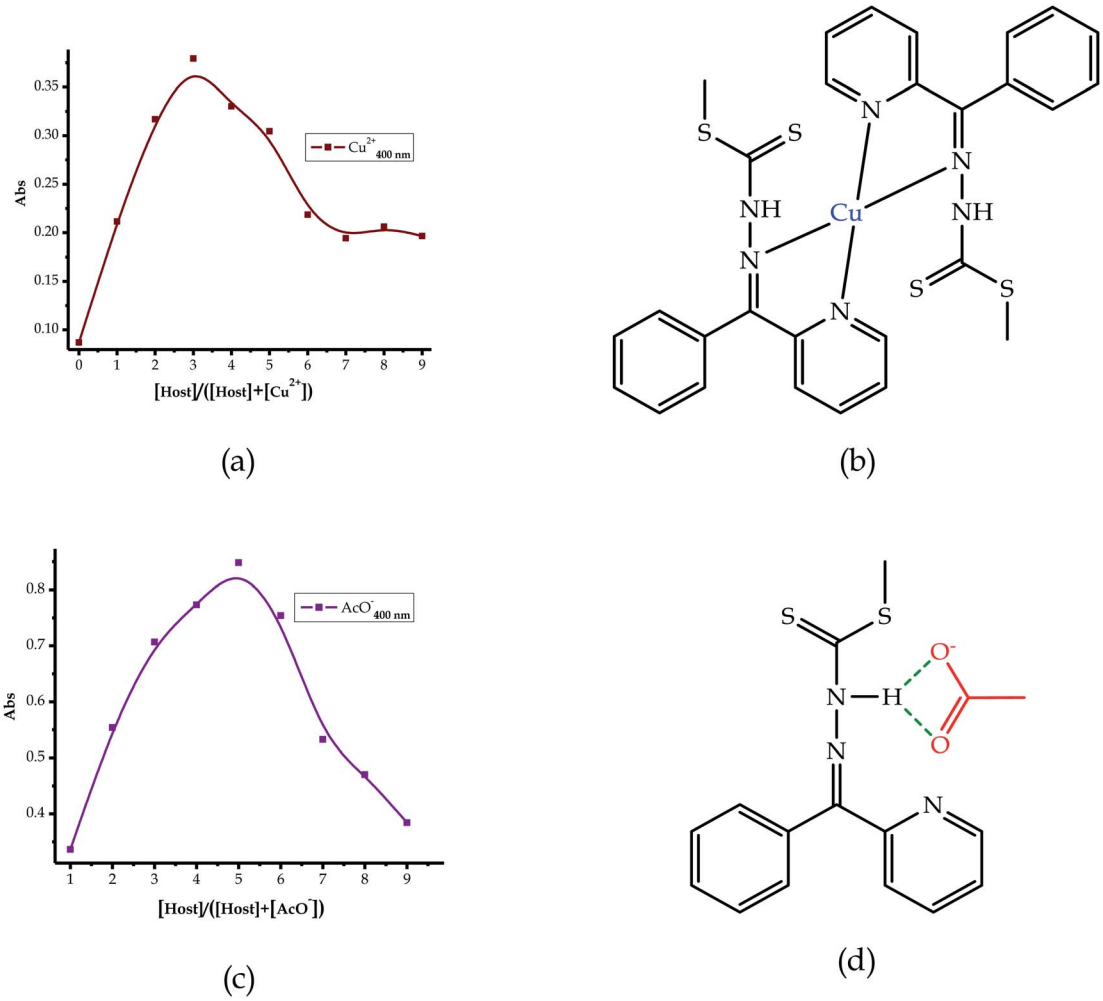

Fig. 7 The proposed interaction and binding modes of **EN** with the cations: (a) Job plot and (b) **EN–Cu**, and anions: (c) Job plot and (d) **EN–AcO**.

at each specific wavelength, as shown in the titration profiles of each complex.[76] Subsequently, the UV-vis titration signals of **EN** with each cation were extrapolated (Fig. S5 and S6†) from the titration profiles, as well as for the anions (Fig. S7†). The detection limits for the cations ranged from 1×10^{-6} M (Sn^{2+}) to 4.5×10^{-9} M (Fe^{2+}), and for the anions the LODs were similarly determined and found to range from 1.5×10^{-7} M (F^-) to 3.8×10^{-8} M (CN^-).

3.4 Theoretical studies of the interaction of EN with the anions

In order to further comprehend the interactions of **EN** with the individual anions (F^-, AcO^-, CN^- and $H_2PO_4^-$), density functional theory (DFT) calculations at [B3LYP/6-31G**] with Spartan'14 were carried out in DMSO. The modelling predicted that the density of the HOMO of **EN** is on the thioic unit, while the LUMO is spread all over the structural skeleton of the sensor (Table 1). However, upon the introduction of the anions, the HOMOs were distributed over the analytes (**EN–F** and **EN–AcO**), while remaining the same for the **EN–CN** and **EN–H_2PO_4** complexes. The HOMO and LUMO levels are calculated to be at −5.81 eV and −2.20 eV, respectively, yielding the energy gap of 3.61 eV, which is centered within the UV region of the spectrum. This is in good agreement with the experimental value of the HOMO–LUMO gap (3.51 eV) and the absorption (maxima) spectrum of **EN** (Fig. 8) in DMSO. However, upon interacting with anions (F^- and AcO^-), the HOMO and LUMO levels, as well as the energy gaps, changed accordingly to 1.67 eV and 3.12 eV, respectively (Table 1). The lower band gap for **EN–F** could also be attributed to the fact that the association constant for the complex is the lowest of the anions used. The HOMO and LUMO of **EN–F** and **EN–AcO** were in both cases concentrated on the guest unit (F^- and AcO^-), while the LUMO was spread across the skeleton of the structure of the probe. Moreover, the HOMO–LUMO levels for **EN–CN** and **EN–H_2PO_4** were comparable in their values and distributions, with the HOMO clouded on the thioic unit, while the LUMO was concentrated along the skeletal frame of the sensor (Table 1). The predictions show that the HOMO–LUMO gaps decreased in all of the complexed states (**EN–F**, **EN–AcO**, **EN–CN** and **EN–H_2PO_4**) compared to that of **EN**, which normally translates into a decrease in the molecular energy and the stability of the complex. Thus, the lowering of

the HOMO–LUMO gap is responsible for the absorption spectra undergoing bathochromic shifts and thus colorimetric changes are observed.

3.5 Solvatochromic studies of EN

The probe was subjected to solvatochromic studies in order to investigate and study the optoelectronic properties of **EN** in relation to solvents of different polarities. Characteristically, it was noticed that many of the chromic shifts shown in the spectra were of a hyperchromic and hypochromic nature, and there were limited bathochromic and hypsochromic shifts (Fig. 8). Most spectra appear to have less intense and broader absorption peaks within the defined spectral range (300 nm to 400 nm), which are in the same region as the main high-energy

Table 1 Frontier molecular orbitals of **EN** and its interactions with anions in DMSO

	HOMO	LUMO	Energy gap (eV)
EN	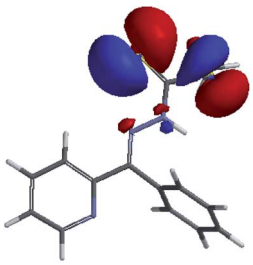 -5.81 eV	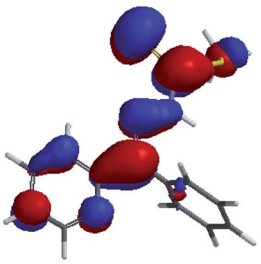 -2.20 eV	**3.61 eV**
EN–F	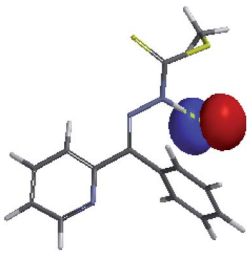 -3.54 eV	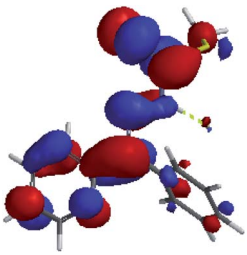 -1.87 eV	**1.67 eV**
EN–AcO	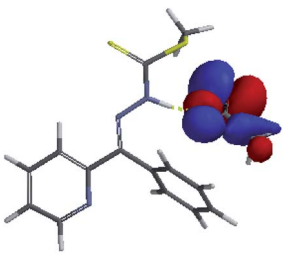 -5.07 eV	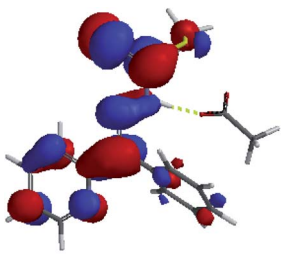 -1.95 eV	**3.12 eV**
EN–CN	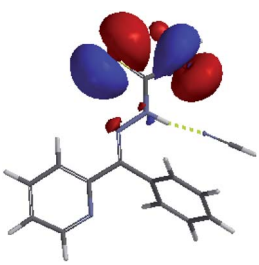 -5.63 eV	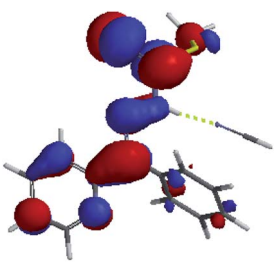 -2.15 eV	**3.48 eV**

Table 1 (*Contd.*)

	HOMO	LUMO	Energy gap (eV)
EN–H_2PO_4	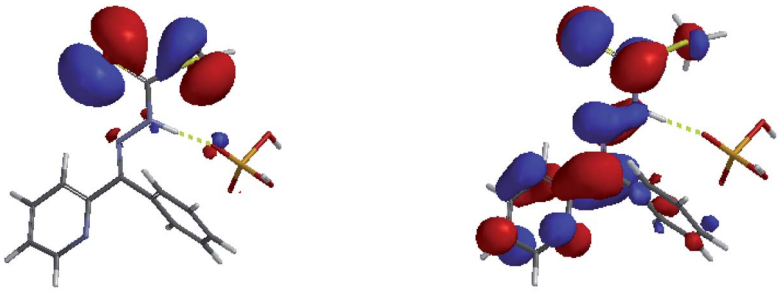 -5.29 eV	-1.94 eV	**3.35 eV**

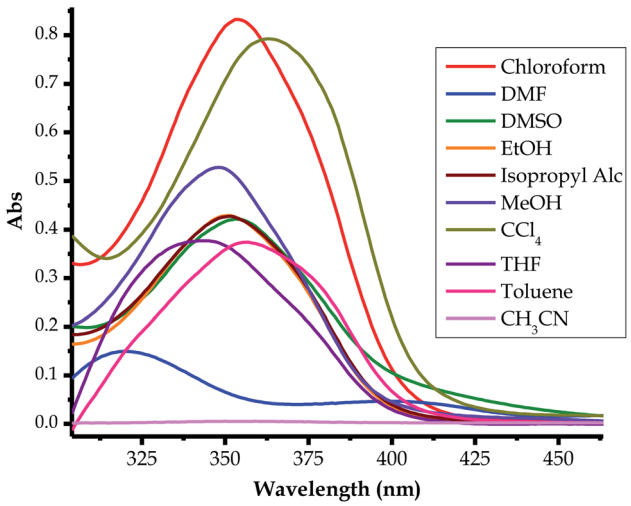

Fig. 8 Absorption spectra of **EN** (1×10^{-5} M) in different solvents for solvatochromism, at room temperature.

intense peak, thus it is hard to assign a specific absorption wavelength for each of these. However, in DMF, the spectrum of **EN** is well defined into two distinctive absorption peaks within the same range as the others (300 nm to 400 nm), with maxima at 314 nm and 400 nm (Fig. 8). In actuality, the spectrum in DMF experiences a bathochromic shift entirely, compared to the rest of the spectra, with the delocalized π–π* transition (at 253 nm in DMSO) red-shifted to 314 nm, while the charge transfer high energy band (at 353 nm in DMSO) is further red-shifted to 400 nm as a broader band. The only major change in this spectrum is the molar extinction coefficient, which experienced a significant decrease, as it undergoes a significant bathochromic shift.

Interestingly, **EN** did not display any noticeable absorption response in CH_3CH in the anticipated functional range, compared with the other solvents. However, the molecular dye has displayed high molar extinction coefficients (hyperchromic effect) in the solvents CCl_4 and $CHCl_3$. The spectral characteristics of typical molecular dye sensitizers which are the most informative about the quantum efficiency are: (i) the molar extinction coefficient and (ii) the broader absorption range. A higher molar extinction coefficient normally enhances photon harvesting, which usually increases the quantum efficiency. Similarly, the broader absorption range of a dye, extended from the visible to near infrared (NIR) regions, increases the

Table 2 UV-visible absorption maxima of **EN** in different solvents[a]

Solvent	λ_{max} (nm)	ε (10^4 L mol^{-1} cm^{-1})	E_{H-L} (eV), $BG^*_{(\lambda_{max})}$	Abs. range (nm_{onset})	BG* range (eV)	E_{H-L} (eV), (calculated)
EtOH	350	4.33	3.54	305–412	4.07–3.01	3.67
MeOH	350	5.33	3.54	300–412	4.07–3.01	
CH_3CN	—	—	—	—	—	—
THF	342	3.81	3.63	290–405	4.28–3.06	3.58
$CHCl_3$	353	8.35	3.51	306–419	4.05–2.95	
$CH_3CHOHCH_3$	350	4.33	3.54	305–412	4.07–3.01	
CCl_4	364	7.97	3.41	314–450	3.95–2.76	
DMSO	353	4.33	3.51	308–437	4.02–2.84	3.61
DMF	319, 403	1.52, 0.50	3.89, 3.07	300–385, 403	4.07–3.22, 3.07	3.61
$C_6H_5CH_3$	356	3.79	3.48	290–425	4.28–2.91	3.49

[a] BG* signifies band gap.

Table 3 Frontier molecular orbitals of **EN** computed in different solvents

Solvent/E_{H-L}	HOMO	LUMO
Vacuum, 3.32 eV	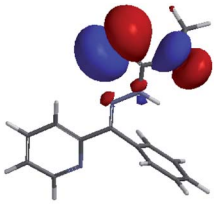 -5.53 eV	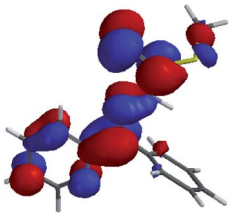 -2.21 eV
Ethanol, 3.67 eV	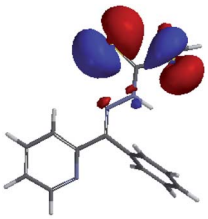 -5.95 eV	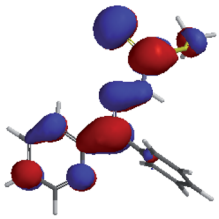 -2.28 eV
DMF, 3.61 eV	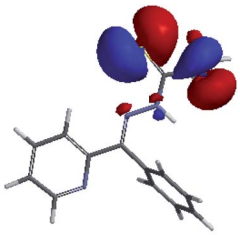 -5.81 eV	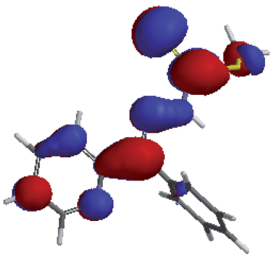 -2.20 eV
THF, 3.58 eV	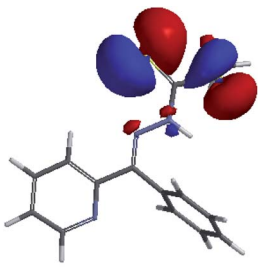 -5.77 eV	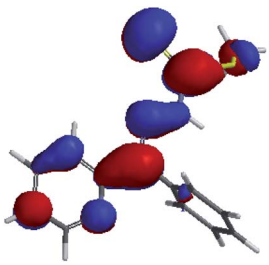 -2.19 eV
DMSO, 3.61 eV	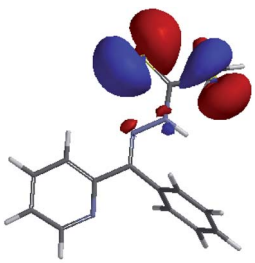 -5.81 eV	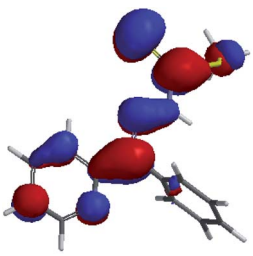 -2.20 eV

Table 3 (*Contd.*)

Solvent/E_{H-L}	HOMO	LUMO
Toluene, 3.49 eV	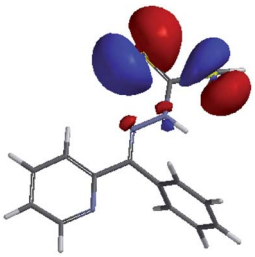 -5.68 eV	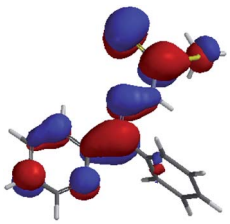 -2.19 eV
Methylene chloride, 3.47 eV	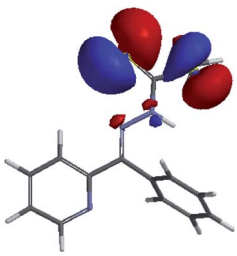 -5.81 eV	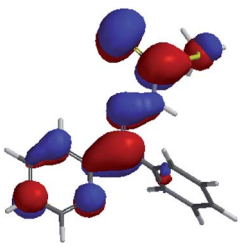 -2.20 eV

functional absorption range, which in turn increases the overall quantum efficiency. Significantly, higher molar extinction coefficients are associated with metal-free dye sensitizers, which lead to the enhancement of the overall incident photon to current quantum efficiency (IPCE) of the cell.[77] In Table 2, the varying molar absorptivities, hence the band gaps (BGs), from different solvents are shown, with CCl_4 and $CHCl_3$ solvents showing the highest extinction coefficients, thus, potentially resulting in a better photon harvester.

3.6 Solvatochromic effect on the optoelectronic properties of EN

The energy band gap (HOMO–LUMO gap) is a determining factor of whether a material can be classified as a conductor (no band gap), semiconductor (≥1 eV) or insulator (≥9 eV). Thus, the optoelectronic properties of **EN** were investigated and studied in the different solvents, both experimentally and theoretically, as shown in Fig. 8. In the solvents used, both the optical and electronic properties have demonstrated that the varying absorption maxima of **EN** are concentrated in the UV region of the spectrum, ranging from 290 nm–450 nm or 4.28 eV–2.76 eV, respectively (Table 2). Moreover, the absorption broadness varied slightly with each solvent, resulting in the different absorption ranges, hence the varying energy gaps. In both cases, the theoretical HOMO–LUMO gaps in different solvents were closely in agreement with experimental values (Table 2). Several methods can be used to determine the band gaps of molecular dyes, both experimentally and theoretically, commonly by applying the expression below (eqn (1)). Conclusively, it can be concluded that **EN** may be a potential dye sensitizer for solar cell applications, however, electronic tuning is highly needed in order to red-shift the optical properties within the visible light region for better photon harvesting.

$$E_{H-L}\ (\text{eV}) = 1240/\lambda\ (\text{nm}) \quad (1)$$

3.7 Theoretical studies of EN

In order to supplement the experimental data above, theoretical simulations (DFT) at the BLYP/6-31G** (Spartan'14 package) level in different solvents were performed to understand the variation and possible geometrical conformation of **EN**. Thus, calculations based on density functional theory (DFT) were applied in order to understand the molecular structure and electron distribution.[78–80] The HOMO was generally distributed on the thioic unit, while the LUMO cloud was mainly distributed across the structural skeleton, including the pyridine ring and the sulfur (=S) unit (Table 3). The magnitudes of the band gaps in each of the solvents obtained theoretically (3.49–3.67 eV) are well within the range of experimental values (3.07–3.89 eV) as displayed in Table 2. Subsequently, the optoelectronic properties of **EN** can be modified to improve its dye sensitizing properties, through the judicious incorporation of functional molecular units, which could shift the absorption maxima to the visible light region, hence adjusting the HOMO–LUMO gap to within the functional wavelengths through quantum confinement.

3.8 Reversibility and reproducibility studies of EN

Since **EN** is a multi-sensor for almost all of the heavy metal cations tested (except Al^{3+} and Cr^{3+}), the reversibility and reproducibility properties of the probe (**EN**) from a complexed state with anions (**EN–F**) were studied using Al^{3+}. Reversibility and reproducibility are normally triggered by the prospect of the sensor undergoing deprotonation when exposed to the excess addition of the anion. Thus, in this case, **EN** was susceptible to deprotonation, since the association with the anions was through hydrogen bonding. The reversibility and reproducibility studies were thus carried out to investigate the likelihood of separating anions from the complexed state (**EN–F**) in the presence of cations (Al^{3+}). The investigation was carried out using **EN–F** interacting with Al^{3+}, however, any other anions (**EN–AcO**, **EN–CN** and **EN–H_2PO_4**) could be used, while aluminium was chosen because it was one of the few metal cations which did not interact with **EN**. It was also ascertained that the interaction between **EN** and the anions was through the –NH group in the structure, which could easily result in the deprotonation process when excess anions were added.

As stated, the studies were carried out by selecting the **EN–F** complex state, with F^- selected from the others. It was suspected that the interaction of **EN** with F^- induced the deprotonation process (eqn (2)) when F^- was in excess (eqn (3)) thereby separating a proton from **EN** (leaving a charged EN^- behind). It was evident that the gradual titration of the complexed state (**EN–F**) with $Al(NO_3)_3 \cdot 9H_2O$ led to the deep yellow colour of **EN–F** being reverted back to the original pale yellow colour of **EN**, as displayed in Fig. 9b. The reversal of **EN–F** to the initial state of **EN** is due to the interaction of F^- with Al^{3+} in the system, which results in the re-protonation of **EN**, thus restoring it to its ground state (pale yellow colour).

At a low F^- concentration (hydrogen bonding):

$$\mathbf{EN}H\ (\mathbf{EN}) + F^- \leftrightarrow [\mathbf{EN}H\text{–}F]^-. \quad (2)$$

With excess F^- concentration (deprotonation):

$$\mathbf{EN}H + 2F^- \leftrightarrow \mathbf{EN}^- + [FHF]^- \quad (3)$$

As a result, the reversal and reproducibility were carried out for several cycles and analysed spectroscopically (Fig. 10a) and colorimetrically (Fig. 10b), which demonstrated the same trend consistently, without much interference in the spectra of **EN** or **EN–F**. The consistency of the spectra during the reversibility and reproducibility process (Fig. 9a) was obviously guided by the interaction between Al^{3+} and F^-, whereby only the addition of Al^{3+} to the deep yellow colour of **EN–F** restored the initial colour of **EN** (Fig. 9b). Notably, the visual reversal and reproducibility occurred simultaneously with the restoration of the absorption spectra of **EN** (Fig. 9a), where the absorption maxima were restored to the initial absorption wavelength. Thus, the quality of the system and its functionality was defined and characterized by the consistency of the restored spectra as compared to the original ones. Subsequently, the reversibility and reproducibility of **EN** was subjected to logic operation functions, where F/Al can be used as modulating input–output entities for predicted combinatorial inhibition (INH) and implication (IMP) logic functions.

3.9 Logic operation studies with F^-/Al^{3+} complementary inputs

The logic operation functions of **EN** were further investigated, prompted by the reproducibility and reversibility properties above. The complexed state (**EN–F**) formed after the molar addition of F^- to **EN** prompted the subsequent restoration titration sequences. However, it is worth noting that the addition of Al^{3+} to **EN** did not yield any interaction signal, either spectrally or colorimetrically (Fig. 11a). This revealed that **EN** has no chemical association with Al^{3+} under the given environmental conditions, thus confirming that the interaction is merely with the complexed state instead. The addition of appropriate combinations of F^- and Al^{3+} as sequential inputs produced the outputs, which are in accordance with complementary IMP/INH logic functions (Fig. 11a). The binary logic

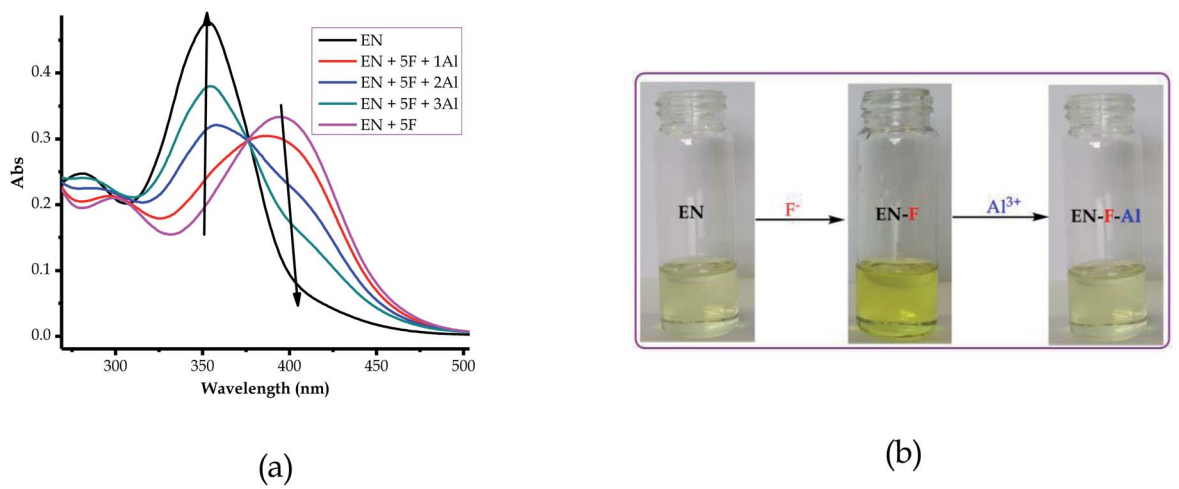

Fig. 9 Reversibility and reproducibility of **EN** (1×10^{-5} M) in DMSO–H_2O (a) spectrally and (b) colorimetrically, .

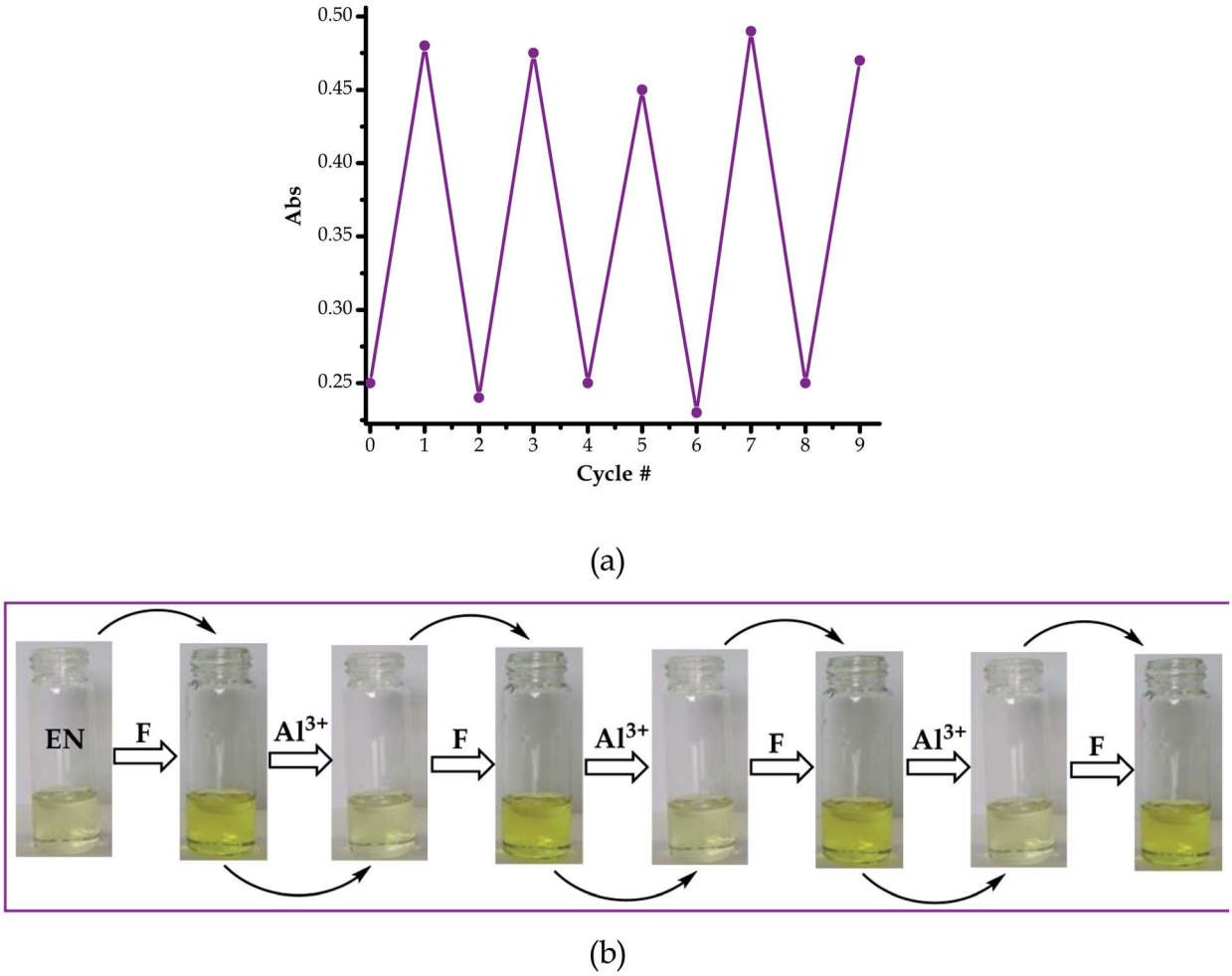

Fig. 10 Reversible cycles and reproducible colorimetric switch of **EN** (1×10^{-5} M, DMSO–H_2O) reversed and reproduced by the addition of F^- and Al^{3+}, respectively, (a) repeating cycles and (b) colorimetric switch of up to 4 cycles.

process is initiated (ON) by the addition of input In1 (F^-) and reversed (OFF) by the input In_2 (Al^{3+}). The spectral changes at 394 nm upon the addition of F^- to **EN** are complementary to an INHIBIT (INH) logic gate, while the reversal of the system to 354 nm upon the molar addition of Al^{3+} are in accordance with an IMPLICATION (IMP) logic gate.

Furthermore, the molar addition of up to 4 equiv. of Al^{3+} to **EN** + 5 equiv. F^- induced a pale yellow colour, concomitant with the spectral change from 394 nm back to 354 nm (Fig. 11a). Specifically, the addition of Al^{3+} has no significant interaction with **EN**, thus these activities are centered around F^- and Al^{3+} within the solution (Fig. 11c), leaving **EN** re-protonated again. The interaction of F^- and Al^{3+} in the solution at the molar level does not interfere with the functions and properties of **EN** by forming solid residues or precipitates, as evidenced by the purity of the spectra. Practically, the ON and OFF reversible processes solely depend on the molar concentrations of the counter cations and anions, electrostatically, in the solution system. The stability of **EN** was further demonstrated when 5 cycles, including colour reversal and restoration changes (Fig. 11a and c), were tested for the F^-/Al^{3+} modulation system, which demonstrated the consistency of the switch and restoration interactions. Moreover, after these 5 cycles, the system could still carry on with more cycles without showing any serious sign of interference, either spectrally and colorimetrically. The IMP (implication) gate, which is an output complementary to an INH (inhibition) input, was therefore proclaimed. In the truth table (Fig. 11b), the corresponding chemical inputs, spectral output signals and their binary encoding are compiled and presented. Thus, these logic gates can be combined in a complementary output circuit whose electronic equivalents are represented in Fig. 11d.

3.10 Detection of F^- in real samples (toothpastes and mouthwash)

The real time application was investigated and carried out to prove and test the effectiveness of **EN** as a sensor towards anions, particularly F^-, by employing quantitative analysis, using two commercial toothpastes and a mouthwash, which are well known to contain standard concentrations of fluoride ions. The preparation of the toothpaste sample solution was prepared according to a known method, as 20 mg ml^{-1} in 1 ml

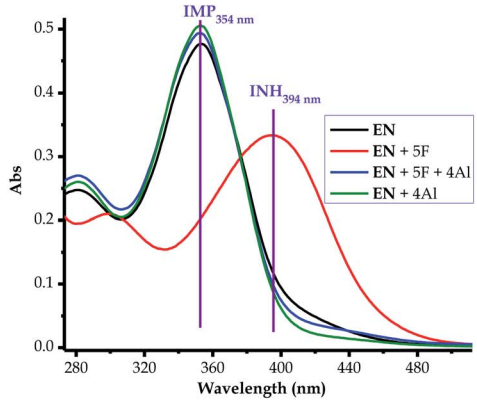

(a)

$In_1(F^-)$	$In_2(Al^{3+})$	IMP_{354nm}	INH_{394nm}
0	0	1	0
1	0	0	1
0	1	1	0
1	1	1	0

(b)

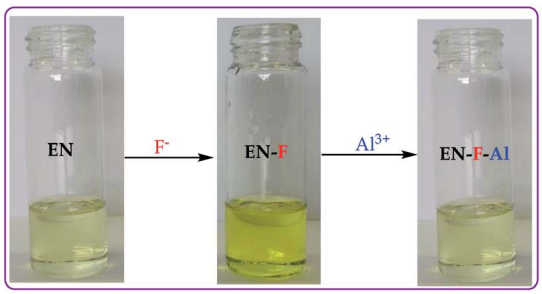

(c)

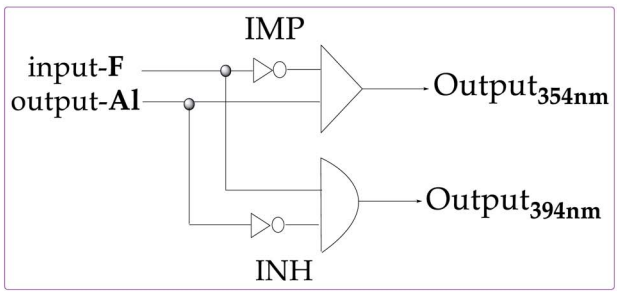

(d)

Fig. 11 (a) Absorption spectra of **EN** (1×10^{-5} M) in DMSO–H_2O with F^- and the molecular logic functions "IMP" (354 nm) and "INH" (394 nm), (b) truth table, (c) reversible and reproducible colorimetric activities and (d) schematic representation of a combinatorial IMP/INH logic circuit.

of H_2O. The two common toothpastes selected were named toothpaste 1 and toothpaste 2 and were used alongside a mouthwash, all of which were readily available in local retailers. The toothpaste aqueous solutions were titrated against **EN** (1×10^{-5} M in DMSO–H_2O) in molar quantities. The sequential molar addition of the mouthwash solution to **EN** resulted in spectral changes, clearly displaying the disappearance of the peak at 354 nm simultaneously with the appearance of a new band at 394 nm (Fig. 12b) through an isosbestic point at 375 nm. The spectral patterns and behaviours of the mouthwash are quite close to those of **EN** *vs.* F^- among the other anion standards used (Fig. 12a). The well-defined spectral response of **EN** *vs.* mouthwash demonstrates the high concentration of fluoride ions in the mouthwash, as compared with the others (toothpaste 1 and toothpaste 2), especially when volumetric quantities were used (40 μL of toothpaste 1 & 40 μL of toothpaste 2 *vs.* 4 μL mouthwash). Consequently, the definition and resolution of the spectra evidenced that the concentration of fluoride ions in the mouthwash was higher than those of toothpaste 1 and toothpaste 2, especially considering the volumetric quantities used in titration. Evidence of the presence of F^- in the toothpastes and mouthwash can be extracted from comparing with the spectra of the standard anions (CN^-, AcO^-, $H_2PO_4^-$ and F^-), and they were closely related and more similar in nature to the spectrum of F^- than those of the other three (Fig. 12a).

Moreover, the titrations of **EN** with toothpaste 1 and toothpaste 2 exhibited similar patterns to those of **EN–F**, whereby they experienced similar spectral shifts (Fig. 12c and d). The molar addition of toothpaste 1 to **EN** resulted in a slight decrease of the peak at 354 nm, concomitant with the appearance of a charge transfer-based band in the region of 400–450 nm (Fig. 12c). The appearance of the charge transfer band is ascribed to the interaction of **EN** with the F^- present in toothpaste 1, which proves the presence of the analyte in the toothpaste. The same method was used in the titration of toothpaste 2 with **EN**, which showed similar patterns to **EN** *vs.* mouthwash and **EN** *vs.* F^-, even though the resolution of the spectrum confirmed that the concentration of fluoride ions is slightly lower in toothpaste 2 (Fig. 12d) as compared with those of toothpaste 1 or the mouthwash. However, the most important take home message is that **EN** could clearly detect fluoride ions in real samples, which is highly vital for the development of real time analytical kits which are suitable for in-field analysis. Thus, **EN** is confirmed to be highly selective and sensitive to F^- and other anions, even when dissolved in water, which is highly ideal for real time analysis.

3.11 Detection of ionic species in saline water samples

The multi-discriminatory power of **EN** prompted the use of the probe in the investigation of the presence of ionic species in

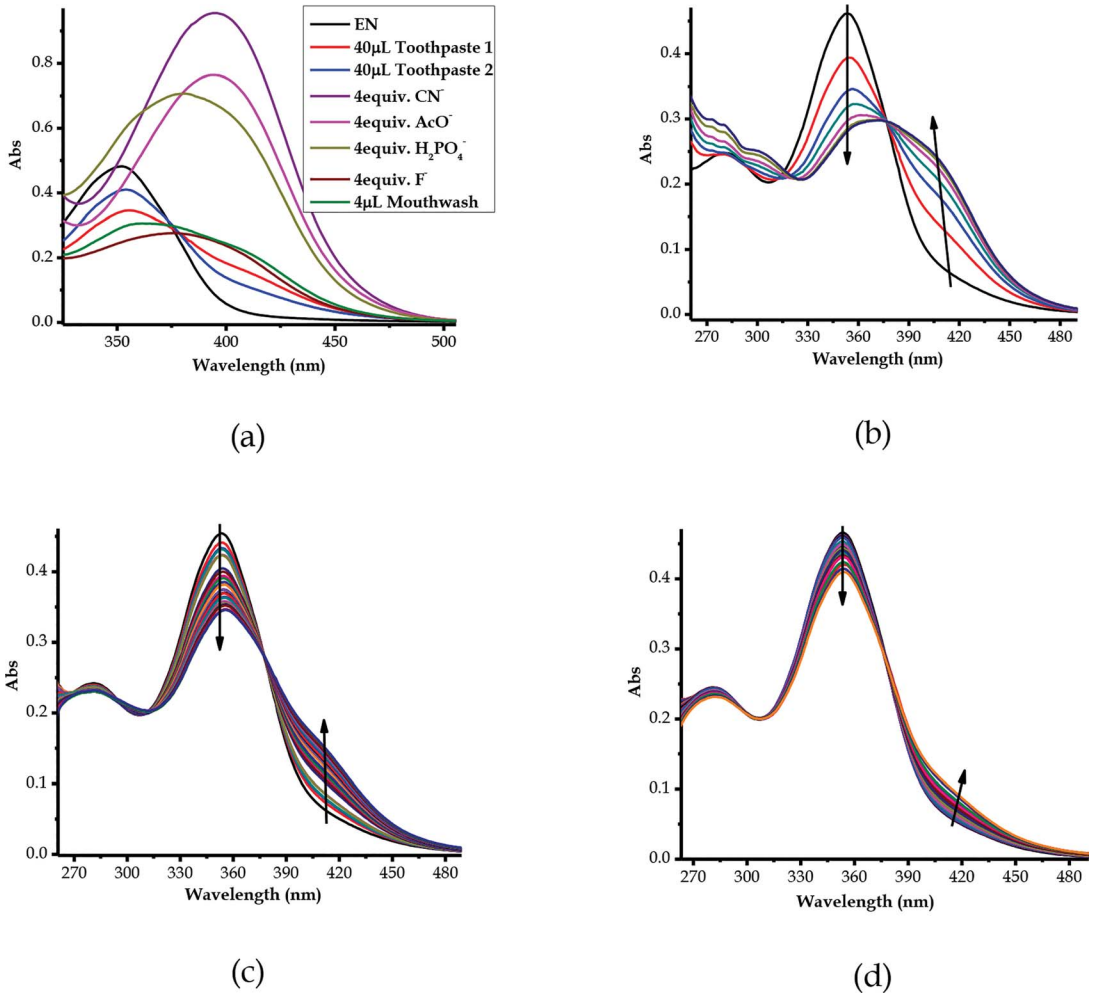

Fig. 12 UV-vis spectra of **EN** (1×10^{-5} M) in DMSO–H_2O: (a) combined absorption spectra of the different anions, (b) mouthwash (4 μL), (c) toothpaste 1 (20 μL) and (d) toothpaste 2 (20 μL) upon the addition of drops of the toothpaste solutions (20g ml^{-1}) in H_2O.

saline water. The samples of saline water (underground water) were collected from Iiputu Village in the Omusati Region, northern Namibia, located at coordinates of 17°38′26.62″ S and 15°38′00.35″ E. This region is known for its prevalent saline underground water at a depth range of 5–100 m.[81] The samples were collected from two adjacent wells, separated by a distance of about 100 m. The wells were (and are still) used as sources of water for household consumption and animals (cattle, goats/sheep, donkeys and others), especially during dry summers and drought seasons. The methodology used was as follows: a sample was collected from each well, then the samples were left for evaporation at room temperature; upon naturally evaporating 85% of the water, the remaining 15% of the aqueous saline concentrate was titrated against **EN** (1×10^{-5} M) in molar equivalents. Consequently, upon the molar addition of the saline solution of Sample 1 to the solution of **EN**, spectral shifts were observed, where the peak at 354 nm experienced a rapid decrease, while a new peak in the region of 400–450 nm appeared with the gradual increase of the addition of the Sample 1solution (Fig. 13a). The same could be said for Sample 2 from the second well, where a hypochromic shift was experienced at 354 nm concomitantly with the appearance of a new peak in the region of 400 to 450 nm (Fig. 13b).

Obviously, it could be confirmed that the two saline samples contain ions of sort, which could possibly be heavy metals, as the spectra resemble the spectra of some of the metal cations used (Fig. 13c). The similarity selection was based on the characteristics of the peak behaviours upon the gradual addition of the analytes, which included the positions of the isosbestic points observed. In addition to the spectral shifts experienced by **EN** upon molar titration with Sample 1 and Sample 2, as explained above, the two isosbestic points for each of these were at 319/376 nm and 320/374 nm, respectively (Fig. 13a and b). It follows that the isosbestic points for Sample 1 and Sample 2 were compatible in their spectral position and shape with those of Fe^{2+}, Pb^{2+}, Sn^{2+} and Fe^{3+} (Fig. 13c). Thus, this could mean that the samples were contaminated with metal fluoride salts, as conclusively suggested in Section 3.10 (Fig. 12), of which the metals could be Fe^{3+} (FeF_3), Fe^{2+} (FeF_2), Pb^{2+} (PbF_2) or Sn^{2+} (SnF_2). However, the geological occurrence and chemical stabilities of some of these metal salt compounds are known in this location, while some of them are rarely known

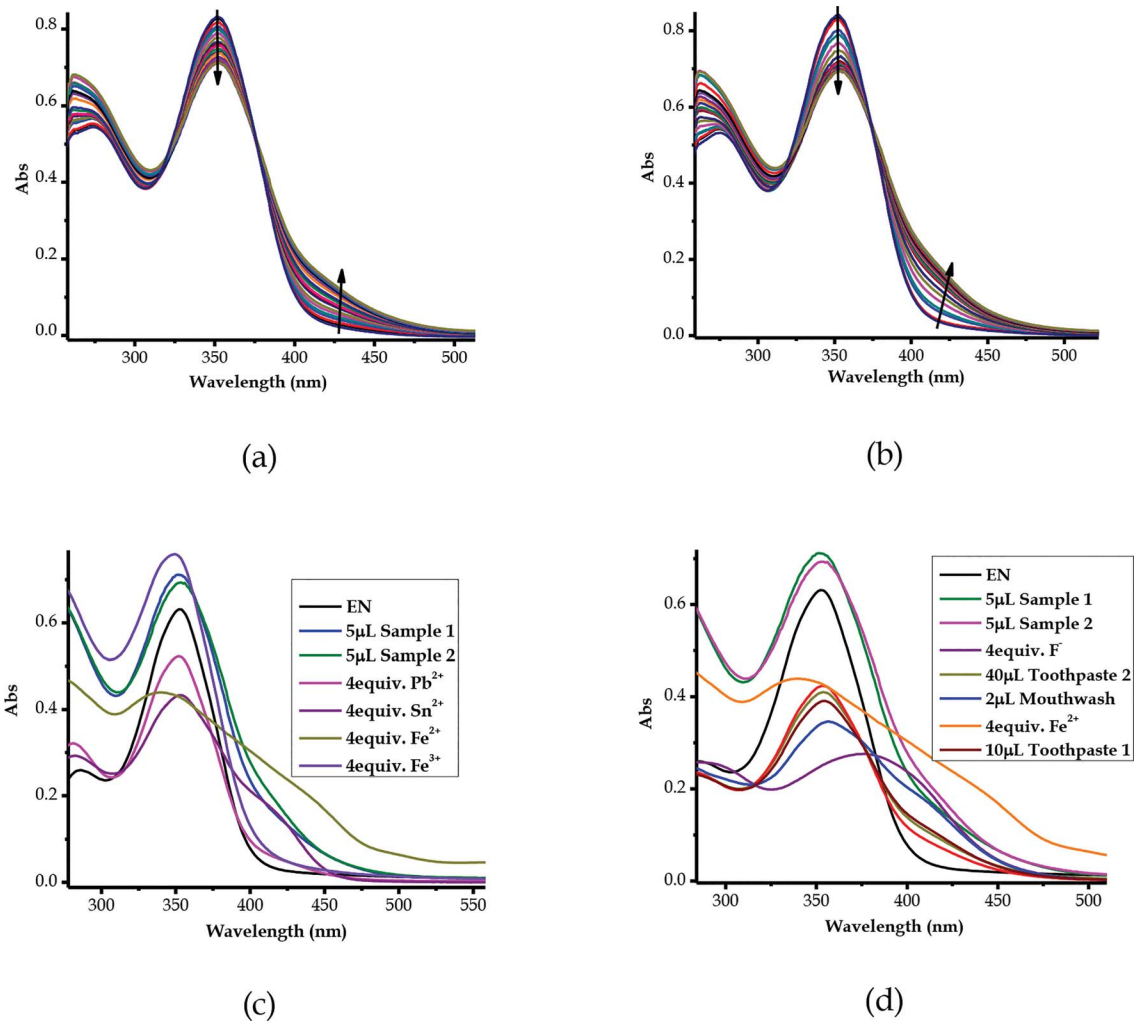

Fig. 13 UV-vis spectra of **EN** (1×10^{-5} M) in DMSO–H_2O with (a) aqueous saline Sample 1 (15 μL) and (b) aqueous saline Sample 2 (15 μL), both in H_2O, (c) combined spectra of the selected cations and the saline samples and (d) combined spectra of the selected real samples as well as the selected ions.

in chemistry (FeF_3 & PbF_2) or to be in this area (FeF_3, PbF_2 and SnF_2). Thus, the identity of the metal salt compounds leaves much to be desired, but FeF_2 and SnF_2 could be in close proximity, both in their spectra shape and position, as well as their occurrence in this location. However, a completely different dimension could be the possibility that the metal salt here is not of a heavy metal cation, but rather of a group metal cation, such as calcium fluoride (CaF_2) or magnesium fluoride (MgF_2), which are all prevalent in this location. Conclusively, it appeared that the two samples from separate wells contained the same type of salinity source, despite coming from two different wells, given the structures and characteristics of their absorption spectra. Another comparison carried out was the mixture of real samples with F^- and Fe^{2+}, which still evidently showed the presence of fluoride ions in both saline samples (Fig. 13d).

3.12 The cross detection studies of EN towards cations

Since **EN** exhibited multi-colorimetric and spectroscopic behaviors, cross detection studies were investigated in order to establish the order in which cations can be detected in the presence of other competitive cations. Thus, sequential titrations were carried out in a single system in order to identify which cations were dominant over the others. The method used a one-off addition of 10 equiv. of the analyte (cation solution) to the sensor (**EN**) solution (1×10^{-5} M) in different sequences, as displayed in Fig. S3a–v†. The one-off addition of 10 equiv. of Ni^{2+} to **EN**, was sequentially followed by another 10 equiv. of Co^{2+} and then 10 equiv. *etc.*, as indicated in Fig. S3a†. The outcome of these sequences was such that changes in the spectral activities were observed accordingly which were specific to cations added (Fig. S3a–v†). Obviously, some of the cations showed superposing power when added to the probe in the presence of other cations. For instance, the addition of Cu^{2+} was immediately noticeable irrespective of the presence of other cations in the solution. Thus, it could be said that the Cu^{2+} ion superposes all other cations present in the solution (Fig. S3c†), followed by Ni^{2+}, as displayed in Fig. S3†. Importantly, most of the cations displayed unique fingerprints in the presence of

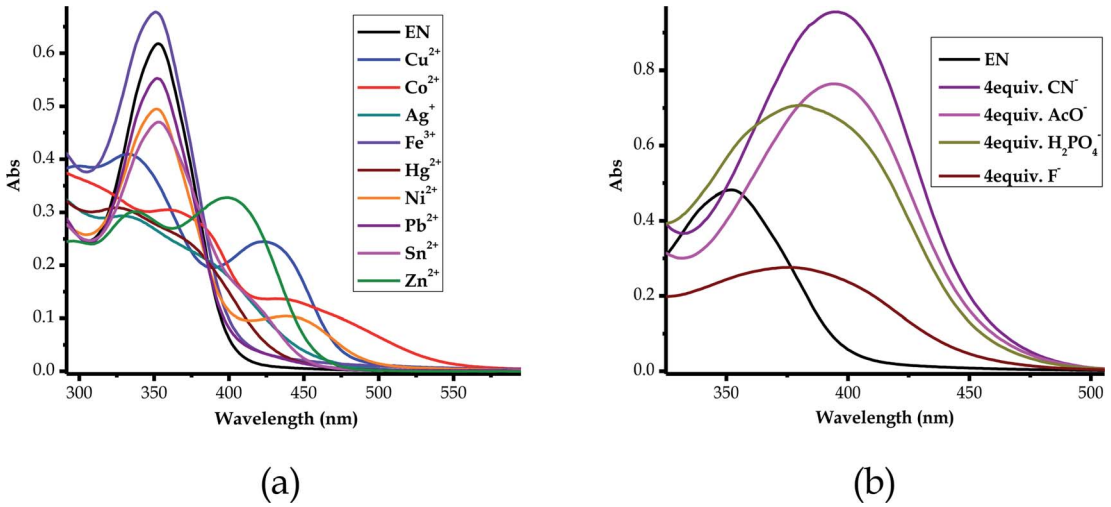

Fig. 14 Combined absorption spectra of **EN** (1×10^{-5} M) in DMSO–H_2O, after titrated with, (a) 2 equiv. of the cations and (b) 4 equiv. of the anions.

other cations, which makes **EN** very versatile in its application towards these cations. Clearly, cations such as Pb^{2+}, Cd^{2+} and Hg^{2+} did have significant impacts upon being added to the sequence of cations in the solution, exhibiting strong association and binding relationships with **EN**. Remarkably, the stability and chemical fingerprints of **EN** upon the addition of sequences of different cations were not affected or denatured by the presence of the different cations, as displayed by the consistency of the spectra.

3.13 Competitive studies of EN with cations and anions

In order to address the selectivity issues, it is vital to establish the competitiveness of anions and cations towards **EN** when all are present in one solution mixture to determine which species predominate over the others. Since **EN** interacts with most of the heavy metal cations, the titration spectra of all of the sensed cations were combined into one graph, upon adding 2 equiv. of each cation. It was established that the affinity of cations towards **EN** was more pronounced for Cu^{2+} and Zn^{2+}, as displayed by their spectra, which differed from the others (Fig. 14a). Importantly, after the addition of 2 equiv. of each, the two spectra were different in their characteristics too, with Zn^{2+} displaying a more enhanced peak centered at 398 nm, while the peak of Cu^{2+} was slightly red-shifted to 422 nm as it experienced a hypochromic shift. The two heavy metals are slightly equally competitive, however, in different ways that are distinguishable from each other in terms of their spectral characteristics, as also displayed by the cross detection studies (Fig. S3†). However, overall, it was established that Cu^{2+} supersedes all other cations when it is present in the solution, as the detection sequence studies revealed. Furthermore, competitive studies were also carried out for the anions, where it become evident that CN^- was more competitive than the others, followed by AcO^- (Fig. 14b), upon the addition of 4 equiv. of each anion. This shows that the association constant for **EN–CN** is highest compared to those of all of the other anions.

4. Conclusion

A multi-colorimetric sensor based on a pyridyl-thioic moiety has been synthesized and its application for discriminating between cations and anions has been studied in a DMSO–H_2O solvent mixture. The probe (**EN**) was able to discriminate between most of the heavy metal cations used, including the most toxic ones (Cd^{2+}, Pb^{2+} and Hg^{2+}) in environmental and physiological setups, however, it was established that it has a higher affinity towards Cu^{2+} and CN^-. Generally, probes for heavy metals such as Cd^{2+} and Pb^{2+} are very rare in the literature, especially in aqueous soluble solvents such as DMSO. In addition, the probe was also able to detect the presence of anions such as CN^- and OH^- in the same solvent mixture, which are very critical in environmental and physiological systems. Furthermore, since colorimetric changes are caused by hydrogen bonding-induced charge transfer upon interacting with anions, the reversibility and reproducibility properties of **EN** in relation to the anions and Al^{3+} were studied. Influenced and guided by the deprotonation process (when F^- is in excess), the molecular logic function properties of **EN** were explored, in which **EN** was found to exhibit complementary IMP/INH logic functions, based on colour and spectral switching (ON/OFF), modulated by F^-/Al^{3+}. Moreover, and more importantly, **EN** was used to detect the presence of F^- in toothpaste products and mouthwash and it turned out that the probe was able to sense fluoride ions in aqueous solutions. The experimental studies were complemented by the theoretical studies, which all turned out to be in agreement with each other. Thus, **EN** not only has the potential of being transformed into a commercial product to develop analytical kits for field work analysis, but has high potential to be a valuable addition to the body of scientific knowledge in the areas of material and analytical chemistry, which are highly desirable.

Conflicts of interest

There are no conflicts to declare.

Acknowledgements

This work was supported by the Department of Chemistry and Biochemistry, University of Namibia, the Center for High Performance Computing, Cape Town, South Africa and the Royal Society–DFiD Africa Capacity Building Initiative for New Materials for a Sustainable Energy Future.

References

1 Y. Ma, P. She, K. Y. Zhang, H. Yang, Y. Qin, Z. Xu, *et al.* Dynamic metal-ligand coordination for multicolour and water-jet rewritable paper, *Nat. Commun.*, 2018, **9**, 3, DOI: 10.1038/s41467-017-02452-w.

2 S. Cao, C. Xu, Z. Guo, Y. Hu, Y. Tang, H. Chen and F. Jiang, Macroscopic urea-functionalized cadmium sulfide material with high visible-light photocatalytic activity for rewritable paper application, *J. Colloid Interface Sci.*, 2017, **500**, 202–211, DOI: 10.1016/j.jcis.2017.04.017.

3 Y. Zhang, A. Ye, Y. Yao and C. Yao, A Sensitive Near-Infrared Fluorescent Probe for Detecting Heavy Metal Ag+ in Water Samples, *Sensors*, 2019, **19**(2), 247.

4 M. Li, H. Gou, I. Al-Ogaidi and N. Wu, Nanostructured sensors for detection of heavy metals: A review, *ACS Sustainable Chem. Eng.*, 2013, **1**(7), 713–723.

5 C. Huang and H. Chang, Selective gold-nanoparticle-based "turn-on" fluorescent sensors for detection of mercury(II) in aqueous solution, *Anal. Chem.*, 2006, **78**(24), 8332–8338, DOI: 10.1021/ac061487i.

6 S. Goswami and R. Chakrabarty, Highly selective colorimetric fluorescent sensor for Pb^{2+}, *Eur. J. Org. Chem.*, 2010, (20), 3791–3795.

7 J. Hatai, S. Pal, G. P. Jose and S. Bandyopadhyay, Histidine based fluorescence sensor detects Hg^{2+} in solution, paper strips, and in cells, *Inorg. Chem.*, 2012, **51**(19), 10129–10135.

8 A. K. Singh, S. Mehtab and A. K. Jain, Selective electrochemical sensor for copper (II) ion based on chelating ionophores, *Anal. Chim. Acta*, 2006, **575**(1), 25–31.

9 A. K. Singh, V. K. Gupta and B. Gupta, Chromium(III) selective membrane sensors based on Schiff bases as chelating ionophores, *Anal. Chim. Acta*, 2007, **585**(1), 171–178.

10 Q. X. Liu, Z. L. Hu and Z. X. Zhao, A new fluorescent-colorimetric chemosensor for cobalt(II) ions based on bis-benzimidazolium salt with three anthraquinone groups, *New J. Chem.*, 2018, **42**(24), 20049–20055.

11 G. Yu, Y. Cao, H. Liu, Q. Wu, Q. Hu, B. Jiang, *et al.* A spirobenzopyran-based multifunctional chemosensor for the chromogenic sensing of Cu^{2+} and fluorescent sensing of hydrazine with practical applications, *Sens. Actuators, B*, 2017, **245**, 803–814.

12 S. Valarmathi, S. Senthil, S. Manjunathan and D. Srividhya, Synthesis and characterization of thiazole based selective chemosensor for copper ions, *Mater. Today: Proc.*, 2020, **33**(5), 2134–2138, http://www.sciencedirect.com/science/article/pii/S2214785320318010.

13 Y. Sun, J. H. Hu, J. Qi and J. B. Li, A highly selective colorimetric and "turn-on" fluorimetric chemosensor for detecting CN-based on unsymmetrical azine derivatives in aqueous media, *Spectrochim. Acta, Part A*, 2016, **167**, 101–105, DOI: 10.1016/j.saa.2016.05.017.

14 L. Wang, W.-T. Li, W.-J. Qu, J.-X. Su, Q. Lin, T.-B. Wei, *et al.* A highly selective fluorescent chemosensor for successive detection of Fe^{3+} and CN^- in pure water, *Supramol. Chem.*, 2017, **29**(7), 489–496.

15 M. Alkış, D. Pekyilmaz, E. Yalçın, B. Aydiner, Y. Dede and Z. Seferoğlu, H-bond stabilization of a tautomeric coumarin-pyrazole-pyridine triad generates a PET driven, reversible and reusable fluorescent chemosensor for anion detection, *Dyes Pigm.*, 2017, **141**, 493–500.

16 V. K. Gupta, N. Mergu, L. K. Kumawat and A. K. Singh, A reversible fluorescence "off-on-off" sensor for sequential detection of aluminum and acetate/fluoride ions, *Talanta*, 2015, **144**, 80–89, DOI: 10.1016/j.talanta.2015.05.053.

17 A. K. Mahapatra, G. Hazra and P. Sahoo, Synthesis of indolo[3,2-b]carbazole-based new colorimetric receptor for anions: A unique color change for fluoride ions, *Beilstein J. Org. Chem.*, 2010, **6**, 12.

18 H. Lin, W. Huang, H. Su and H. Lin, An efficient novel receptor for sensing acetate, *J. Inclusion Phenom. Macrocyclic Chem.*, 2011, **70**(1–2), 129–133.

19 W. T. Gong, B. Gao, S. Bao, J. W. Ye and G. L. Ning, Selective "naked-eye" sensing of acetate ion based on conformational flexible amide-pyridinium receptor, *J. Inclusion Phenom. Macrocyclic Chem.*, 2012, **72**(3–4), 481–486.

20 C. Olivier, Z. Grote, E. Solari, R. Scopelliti and K. Severin, A self-assembled receptor for the recognition of phosphate and acetate anions in neutral aqueous solution, *Chem. Commun.*, 2007, **39**, 4000–4002.

21 S. Erdemir, O. Kocyigit, O. Alici and S. Malkondu, "Naked-eye" detection of F^- ions by two novel colorimetric receptors, *Tetrahedron Lett.*, 2013, **54**(7), 613–617, DOI: 10.1016/j.tetlet.2012.11.138.

22 K. K. Upadhyay, A. Kumar, R. K. Mishra, T. M. Fyles, S. Upadhyay and K. Thapliyal, Reversible colorimetric switching of thiophene hydrazone based on complementary IMP/INH logic functions, *New J. Chem.*, 2010, **34**(9), 1862–1866.

23 R. L. Mattison, A. A. Bowyer and E. J. New, Small molecule optical sensors for nickel: The quest for a universal nickel receptor, *Coord. Chem. Rev.*, 2020, **425**, 213522.

24 V. K. Gupta, R. N. Goyal and R. A. Sharma, Anion recognition using newly synthesized hydrogen bonding disubstituted phenylhydrazone-based receptors: Poly(vinyl chloride)-based sensor for acetate, *Talanta*, 2008, **76**(4), 859–864.

25 A. E. Hargrove, S. Nieto, T. Zhang, J. L. Sessler and E. V. Anslyn, Artificial receptors for the recognition of phosphorylated molecules, *Chem. Rev.*, 2011, **111**(11), 6603–6782.

26 A. Satheshkumar, E. H. El-Mossalamy, R. Manivannan, C. Parthiban, L. M. Al-Harbi, S. Kosa, *et al.* Anion induced azo-hydrazone tautomerism for the selective colorimetric sensing of fluoride ion, *Spectrochim. Acta, Part A*, 2014, **128**, 798–805, DOI: 10.1016/j.saa.2014.02.200.

27 H. L. Zhang, T. B. Wei, W. T. Li, W. J. Qu, Y. L. Leng, J. H. Zhang, *et al.* Phenazine-based colorimetric and fluorescent sensor for the selective detection of cyanides based on supramolecular self-assembly in aqueous solution, *Spectrochim. Acta, Part A*, 2017, **175**, 117–124, DOI: 10.1016/j.saa.2016.12.022.

28 X. Cheng, H. Li, F. Zheng, Q. Lin, Y. Zhang, H. Yao, *et al.* A pillar[5]arene-based cyanide sensor bearing on a novel cyanide-induced self-assemble mechanism, *Dyes Pigm.*, 2016, **127**, 59–66, DOI: 10.1016/j.dyepig.2015.12.021.

29 D. Maity and T. Govindaraju, Highly selective colorimetric chemosensor for Co^{2+}, *Inorg. Chem.*, 2011, **50**(22), 11282–11284.

30 E. Hamidi-Asl, I. Palchetti, E. Hasheminejad and M. Mascini, A review on the electrochemical biosensors for determination of microRNAs, *Talanta*, 2013, **115**, 74–83.

31 G. Chen, F. Song, X. Xiong and X. Peng, Fluorescent Nanosensors Based on Fluorescence Resonance Energy Transfer (FRET), *Ind. Eng. Chem. Res.*, 2013, **52**, 11228–11245, DOI: 10.1021/ie303485n.

32 Y. Li, H. Lin and H. Lin, Ratiometric and selective fluorescent sensor for F^- based on intramolecular charge transfer (ICT), *J. Fluoresc.*, 2010, **20**(6), 1299–1305.

33 N. Singla, V. S. Bhadram, C. Narayana and P. Chowdhury, White light generation by carbonyl based indole derivatives due to proton transfer: An efficient fluorescence sensor, *J. Phys. Chem. A*, 2013, **117**(13), 2738–2752.

34 F. Ding, S. Chen and H. Wang, Computational study of ferrocene-based molecular frameworks with 2,5-diethynylpyridine as a chemical bridge, *Materials*, 2010, **3**(4), 2668–2683.

35 S. Namuangruk, R. Fukuda, M. Ehara, J. Meeprasert, T. Khanasa, S. Morada, *et al.* D–D–π–A-Type Organic Dyes for Dye-Sensitized Solar Cells with a Potential for Direct Electron Injection and a High Extinction Coefficient: Synthesis, Characterization, and Theoretical Investigation, *J. Phys. Chem. C*, 2012, **116**(49), 25653–25663, DOI: 10.1021/jp304489t.

36 S. Guha, F. S. Goodson, L. J. Corson and S. Saha, Boundaries of Anion/Naphthalenediimide Interactions: From Anion–π Interactions to Anion-Induced Charge-Transfer and Electron-Transfer Phenomena, *J. Am. Chem. Soc.*, 2012, **134**(33), 13679–13691.

37 K. J. Winstanley, S. J. Allen and D. K. Smith, Encapsulated binding sites—synthetically simple receptors for the binding and transport of HCl, *Chem. Commun.*, 2009, (28), 4299–4301.

38 P. A. Gale, Anion receptor chemistry, *Chem. Commun.*, 2011, **47**(1), 82–86, http://xlink.rsc.org/?DOI=C0CC00656D.

39 V. Reena, S. Suganya and S. Velmathi, Synthesis and anion binding studies of azo-Schiff bases: Selective colorimetric fluoride and acetate ion sensors, *J. Fluorine Chem.*, 2013, **153**, 89–95, DOI: 10.1016/j.jfluchem.2013.05.010.

40 D. Faye, J.-P. P. Lefevre, J. A. Delaire and I. Leray, A selective lead sensor based on a fluorescent molecular probe grafted on a PDMS microfluidic chip, *J. Photochem. Photobiol., A*, 2012, **234**, 115–122, DOI: 10.1016/j.jphotochem.2012.01.006.

41 Y. Hu, Y. Li, J. F. Joung, J. Yin, S. Park, J. Yoon, *et al.* Iridium complex bearing urea groups as a phosphorescent chemosensor for chiral anion recognition, *Sens. Actuators, B*, 2017, **241**, 224–229.

42 X. Wu, Q. Niu and T. Li, A novel urea-based "turn-on" fluorescent sensor for detection of Fe^{3+}/F^- ions with high selectivity and sensitivity, *Sens. Actuators, B*, 2016, **222**, 714–720, http://linkinghub.elsevier.com/retrieve/pii/S0925400515302756.

43 S. Mukherjee, S. Talukder, S. Chowdhury, P. Mal and H. Stoeckli-Evans, Synthesis , structure and sensing behavior of hydrazone based chromogenic chemosensors for Cu^{2+} in aqueous environment, *Inorg. Chim. Acta*, 2016, **450**, 216–224, DOI: 10.1016/j.ica.2016.05.049.

44 V. K. Gupta, A. K. Singh, S. Bhardwaj and K. R. Bandi, Biological active novel 2,4-dinitro phenyl hydrazones as the colorimetric sensors for selective detection of acetate ion, *Sens. Actuators, B*, 2014, **197**, 264–273, DOI: 10.1016/j.snb.2014.03.006.

45 V. Uahengo, B. Xiong, P. Cai, L. S. L. S. Daniel, L. Rhyman and P. Ramasami, Chromogenic signaling of water traces by 1,8-naphthalohydrazone-anion complex in organic solvents, *Anal. Chem. Res.*, 2016, **8**, 1–8, DOI: 10.1016/j.ancr.2016.03.001.

46 S. Shanmugaraju and P. S. Mukherjee, π-Electron rich small molecule sensors for the recognition of nitroaromatics, *Chem. Commun.*, 2015, **51**, 16014–16032, DOI: 10.1039/c5cc07513k.

47 A. K. Ray, *Org. Mater.*, 2017, **52.1**, 1281–1310.

48 O. A. Blackburn, B. J. Coe, J. Fielden, M. Helliwell, J. J. W. McDouall and M. G. Hutchings, Nickel(II) and palladium(II) complexes of azobenzene-containing ligands as dichroic dyes, *Inorg. Chem.*, 2010, **49**(20), 9136–9150.

49 Z. Xu, Y. Xiao, X. Qian, J. Cui and D. Cui, Ratiometric and Selective Fluorescent Sensor for Cu^{II} Based on Internal Charge Transfer (ICT), *Org. Lett.*, 2005, **7**(Ii), 1053–1056.

50 S. Y. Lee, S. Y. Kim, J. A. Kim and C. Kim, A dual chemosensor: Colorimetric detection of Co^{2+} and fluorometric detection of Zn^{2+}, *J. Lumin.*, 2016, **179**, 602–609.

51 J. Cheng, E. Yang, P. Ding, J. Tang, D. Zhang, Y. Zhao, *et al.* Two rhodamine based chemosensors for Sn^{4+} and the application in living cells, *Sens. Actuators, B*, 2015, **221**, 688–693.

52 J. Naimhwaka and V. Uahengo, A naphthoquinone based colorimetric probe for real-time naked eye detection of biologically important anions including cyanide ions in tap water: experimental and theoretical studies, *RSC Adv.*, 2019, **9**(65), 37926–37938.

53 M. Orojloo and S. Amani, Naked-eye detection of cyanide ions in aqueous media based on an azo-azomethine chemosensor, *C. R. Chim.*, 2017, **20**(4), 415–423, DOI: 10.1016/j.crci.2016.07.003.

54 S. Y. Gwon, B. A. Rao, H. S. Kim, Y. A. Son and S. H. Kim, Novel styrylbenzothiazolium dye-based sensor for mercury, cyanide and hydroxide ions, *Spectrochim. Acta, Part A*, 2015, **144**, 226–234, DOI: 10.1016/j.saa.2015.02.094.

55 K. Jakusová, J. Donovalová, M. Cigáň, M. Gáplovský, V. Garaj and A. Gáplovský, Isatinphenylsemicarbazones as efficient colorimetric sensors for fluoride and acetate anions - Anions induce tautomerism, *Spectrochim. Acta, Part A*, 2014, **123**, 421–429.

56 P. Tisovsk, M. Horv, K. Csicsai, J. Donovalov and J. Filo, Isatin-1,8-Naphthalimide Hydrazones: A Study of Their Sensor and ON/OFF Functionality, *Molecules*, 2019, **24**(3), 397.

57 Y. K. Shtaitz, M. I. Savchuk, D. S. Kopchuk, O. S. Taniya, S. Santra, G. V. Zyryanov, A. I. Suvorova, V. L. Rusinov and O. N. Chupakhin, Efficient Synthesis of Methyl 6-(6-Aryl-1,2,4-triazin3-yl)pyridine-2-carboxylates, *Russian Journal of Organic Chemistry*, 2020, **56**(3), 548–551, DOI: 10.1134/S1070428020030306.

58 W. Li, H. Li, H. Li, M. Chen, Y. Shi and J. Lang, 1,4-Bis(2-(pyridin-4-yl)vinyl)naphthalene and Its Zinc(ii) Coordination Polymers: Synthesis, Structural Characterization, and Selective Luminescent Sensing of Mercury(ii) Ion, *Cryst. Growth Des.*, 2017, **17**(7), 3948–3959.

59 A. Shylaja, S. R. Rubina, S. S. Roja and R. R. Kumar, Novel blue emissive dimethylfuran tethered 2-aminopyridine-3-carbonitrile as dual responsive fluorescent chemosensor for Fe^{3+} and picric acid in nanomolar detection limit, *Dyes Pigm.*, 2020, **174**, 108062, DOI: 10.1016/j.dyepig.2019.108062.

60 M. N. Arshad, M. M. Rahman, A. M. Asiri, T. R. Sobahi and S.-H. Yu, *RSC Adv.*, 2015, **5**, 81275–81281.

61 M. R. Ganjali, M. Rezapour, S. Rasoolipour, P. Norouzi and M. Adib, Application of pyridine-2-carbaldehyde-2-(4-methyl- 1,3-benzo thiazol-2-yl)hydrazone as a neutral ionophore in the construction of a novel Er(III) sensor, *J. Braz. Chem. Soc.*, 2007, **18**(2), 352–358, DOI: 10.1590/S0103-50532007000200016.

62 S. Mamour, D. Mayoro, T. E. Ibrahima, G. Mohamed, B. A. Hamady and J. Ellena, {1-[1-(2- Hydroxyphenyl) ethylidene]-2-(pyridin-2-yl-κ N)hydrazine-κ 2 N ′, O }{1-[1-(2-oxidophenyl)ethylidene]-2-(pyridin-2-yl-κ N)hydrazine-κ 2 N ′, O }nickelate(II) nitrate hemihydrate, *Acta Cryst.*, 2018, **E74**, 642–645.

63 R. Šandrik, P. Tisovský, K. Csicsai, J. Donovalová, G. Martin, R. Sokolík, J. Filo and A. Gáplovský, ON/OFF Photostimulation of Isatin Bipyridyl Hydrazones: Photochemical and Spectral Study, *Molecules*, 2019, **24**, 2668, DOI: 10.3390/molecules24142668.

64 J. K.-H. Wong, M. H. Todd and P. J. Rutledge, Recent Advances in Macrocyclic Fluorescent Probes for Ion Sensing, *Molecules*, 2017, **22**(2), 200, DOI: 10.3390/molecules22020200.

65 L. Zhu, L. Zhang and A. H. Younes, Mini review: Fluorescent heteroditopic ligands of metal ions, *Supramol. Chem.*, 2009, **21**(3–4), 268–283.

66 B. I. Kharisov, P. E. Martínez, V. M. Jiménez, O. V. Kharissova and B. N. Martínez, Recent advances on ditopic ligands, *J. Coord. Chem.*, 2010, **63**(1), 1–25.

67 Z. Dong, X. Tian, Y. Chen, J. Hou, Y. Guo, J. Sun, *et al.* A highly selective fluorescent chemosensor for Hg^{2+} based on rhodamine B and its application as a molecular logic gate, *Dyes Pigm.*, 2013, **97**(2), 324–329, DOI: 10.1016/j.dyepig.2013.01.002.

68 V. Uahengo, B. Xiong, N. Zhou, P. Cai, K. Hu and G. Cheng, Synthesis of a phenylhydrazone-based colorimetric anion sensor with complementary IMP/INH logic functions, *Chin. J. Chem.*, 2012, **30**(8), 1702–1708.

69 I. Pecnikaj, D. Minudri, L. Otero, F. Fungo, M. Cavazzini, S. Orlandi, *et al.* Fluorous molecules for dye-sensitized solar cells: Synthesis and properties of di-branched, di-anchoring organic sensitizers containing fluorene subunits, *New J. Chem.*, 2017, **41**(15), 7729–7738.

70 Z. Lin, Y. Ma, X. Zheng, L. Huang, E. Yang, C. Wu, *et al.* #Amide-based diarylmaleimide derivatives and polymers: Highly selective and ratiometric fluorescence sensing for anions, *Dyes Pigm.*, 2015, **113**, 129–137, DOI: 10.1016/j.dyepig.2014.08.006.

71 A. Venkateswararao, K. R. J. Thomas, C. P. Lee and K. C. Ho, Synthesis and characterization of organic dyes containing 2,7-disubstituted carbazole π-linker, *Tetrahedron Lett.*, 2013, **54**(30), 3985–3989, DOI: 10.1016/j.tetlet.2013.05.069.

72 A. Mishra, M. K. R. Fischer and P. Büuerle, Metal-free organic dyes for dye-sensitized solar cells: from structure: property relationships to design rules , *Angew. Chem., Int. Ed.*, 2009, **48**(14), 2474–2499.

73 T. Gatti, N. Manfredi, C. Boldrini, F. Lamberti, A. Abbotto and E. Menna, A D-π-A organic dye – Reduced graphene oxide covalent dyad as a new concept photosensitizer for light harvesting applications, *Carbon*, 2017, **115**, 746–753, DOI: 10.1016/j.carbon.2017.01.081.

74 H. Tan, D. Cai, Z. Liu, F. Zhong, H. Lv, X. Zhang, *et al.* Effects of 2-hexylthiophene on the performance of triphenylamine based organic dye for dye-sensitized solar cells, *Synth. Met.*, 2016, **214**, 56–61, DOI: 10.1016/j.synthmet.2016.01.019.

75 V. Uahengo, B. Xiong, N. Zhou, P. Cai, K. Hu and G. Cheng, Synthesis of a phenylhydrazone-based colorimetric anion sensor with complementary IMP/INH logic functions, *Chin. J. Chem.*, 2012, **30**(8).

76 V. K. Gupta, A. K. Singh and N. Gupta, Colorimetric sensor for cyanide and acetate ion using novel biologically active hydrazones, *Sens. Actuators, B*, 2014, **204**, 125–135, DOI: 10.1016/j.snb.2014.07.029.

77 M. Ryan, Progress in ruthenium complexes for dye sensitised solar cells, *Platinum Met. Rev.*, 2009, **53**(4), 216–218.

78 B. J. Lynch, P. L. Fast, M. Harris and D. G. Truhlar, Adiabatic connection for kinetics, *J. Phys. Chem. A*, 2000, **104**(21), 4811–4815.

79 A. D. Becke, Density-functional thermochemistry. III. The role of exact exchange, *J. Chem. Phys.*, 1993, **98**(7), 5648–5652.

80 C. Lee, W. Yang and R. G. Parr, Development of the Colle-Salvetti correlation-energy formula into a functional of the electron density, *Phys. Rev. B: Condens. Matter Mater. Phys.*, 1988, **37**(2), 785–789.

81 K. Dierkes, *Groundwater Investigations in the Cuvelai-Etosha Basin; Implementation of a Hydrocensus in Parts of the Oshana, Omusati, Oshikoto andOhangwena Regions; Technical Cooperation Project BGR/DWAF*, 2011, 10, https://www.google.com/url?sa=t&rct=j&q=&esrc=s&source=web&cd=&cad=rja&uact=8&ved=2ahUKEwjf-JqK8svyAhUEQUEAHSpEDQMQFnoECAMQAQ&url=https%3A%2F%2Fwww.bgr.bund.de%2FEN%2FThemen%2FWasser%2FProjekte%2Fabgeschlossen%2FTZ%2FNamibia%2Fceb_techn_rep_1c.pdf%3F__blob%3DpublicationFile%26v%3D2&usg=AOvVaw3sICc3DUEKwbQ36X0DohHn.